D3.2 Report on heat transfer modelling and circulation within the borehole

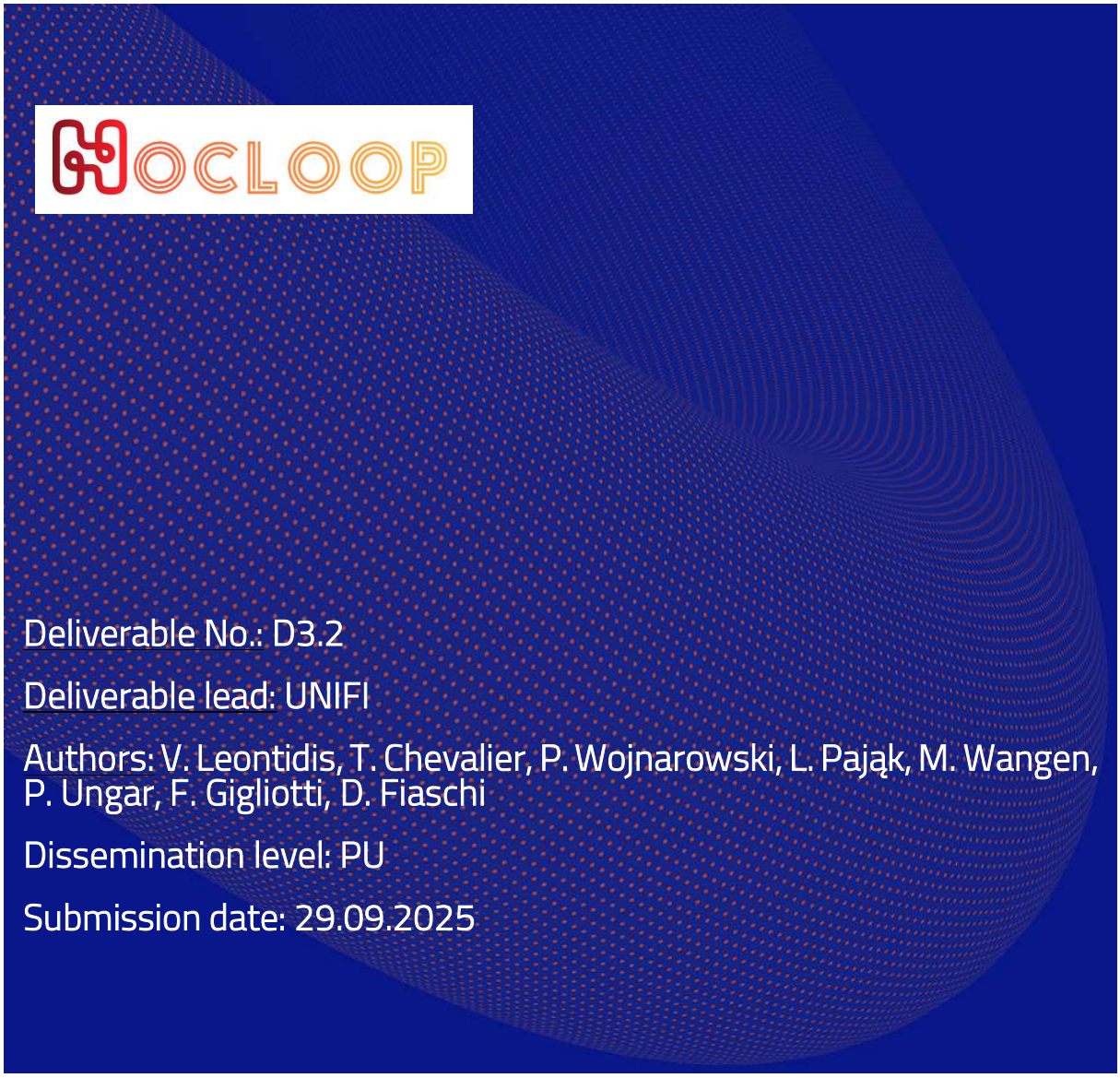

Deliverable No.: D3.2

Deliverable lead: UNIFI

Authors: V. Leontidis, T. Chevalier, P. Wojnarowski, L. Pająk, M. Wangen, P. Ungar, F. Gigliotti, D. Fiaschi

Dissemination level: PU

Submission date: 29.09.2025

Funded by the European Union. Views and opinions expressed are however those of the author(s) only and do not necessarily reflect those of the European Union or CINEA. Neither the European Union nor the granting authority can be held responsible for them.

PROJECT INFORMATION

PROJECT ACRONYM	HOCLOOP
Call ID	HORIZON- CL5-2021-D3-03-15
Project title	A circular by design environmentally friendly geothermal energy solution based on a horizontal closed loop - HOCLOOP
Grant Agreement No	101083558
Start of Project	01.10.2022
Project Duration	42 Months
Type of Action	HORIZON Research and Innovation Actions
Coordinator	IFE

DOCUMENT INFORMATION

Deliverable No.	D3.2
Work Package	WP3
Deliverable Lead	UNIFI
Deliverable Authors	V. Leontidis (IFPEN), T. Chevalier (IFPEN), P. Wojnarowski (AGH), L. Pająk (AGH), M. Wangen (IFE), P. Ungar (UNIFI), F. Gigliotti (UNIFI), D. Fiaschi (UNIFI)
Issue	1/1
Due date	30.09.2025
Submission date	29.09.2025
Dissemination level[1]	PU

[1] Dissemination level: **PU** = Public, **SEN** = Sensitive, **R-UE/EU-R** = EU classified, **C-UE/EU-C** = EU classified, **S-UE/EU-S** – EU classified

This project has received funding from the European Union's Horizon Europe research and innovation program under grant agreement No 101083558

Nature[2]	R
Copyright	© 2023 Consortium

DOCUMENT HISTORY

DATE	VERSION	MODIFIED BY	COMMENT
16.09.2025	0.1	V. Leontidis (IFPEN), T. Chevalier (IFPEN), P. Wojnarowski (AGH), L. Pająk (AGH), M. Wangen (IFE), P. Ungar (UNIFI), D Fiaschi (UNIFI)	First draft
16.09.2025	0.2	Mario Silva (IFE)	First internal revision
16.09.2025	0.3	Mario Silva	Distributed for peer review
22.09.2025	0.4	Virginie Harcouët-Menou (VITO), Hung Pham (TUD)	Reviewer's comments
29.09.2025	1.0	Federico Gigliotti (UNIFI), P. Ungar (UNIFI), D Fiaschi (UNIFI)	Review addressed
29.09.2025	2.0	Mario Silva (IFE)	Final version

[2] Nature of the deliverable: deliverable: **R** = Document, report; **DEM** – Demonstrator, pilot, prototype; **DEC** – Websites, patent, filings, videos etc; **DATA** – data sets, microdata, etc; **DMP** – Data Management Plan; **ETHICS**; **SECURITY**; **OTHER**

This project has received funding from the European Union's Horizon Europe research and innovation program under grant agreement No 101083558

TABLE OF CONTENTS

PROJECT INFORMATION 2
DOCUMENT INFORMATION 2
DOCUMENT HISTORY 3
TABLE OF CONTENTS 4
LIST OF TABLES 6
LIST OF FIGURES 6
LIST OF ABBREVIATIONS 8
EXECUTIVE SUMMARY 9
Scope of the deliverable 9
Main conclusions 9
1. Introduction 10
1.1. General Introduction to WP3 10
1.2. Objective and structure of this deliverable 10
2. Analysis of Key Aspects 11
2.1. Assessment of EoS for single component (pure) fluids 11
3. Methodology 16
3.1. Developed Numerical Tools for Compressible Fluids 16
3.1.1. BHEModel2.0 (UNIFI) 16
3.1.2. GWellFM (IFPEN) 16
3.1.3. GTW (IFE) 16
3.2. Case studies 17
3.2.1. Model validation 17
3.2.2. France 17
3.2.3. Italy 19
3.2.4. Poland 19
4. Results 21
4.1. Model validation 21
4.2. French Case Study 21
4.3. Italian case study 23
4.4. Polish case study 24
5. Conclusions 27
6. References 29
7. Annex I: Assessment of EoS for Mixture Modelling 32
7.1. Miscible Fluids Mixture Model 33
7.1.1. General Introduction 33
7.1.2. UNIFI Modelling Approach 33
7.2. Non-Miscible Fluids Mixture Model 35

This project has received funding from the European Union's Horizon Europe research and innovation program under grant agreement No 101083558

8. Annex II: Analysis of Heat Transfer Coefficients for Supercritical Flows 37
8.1. Heat Transfer Deterioration (HTD) 40
8.1.1. Heat Transfer Coefficient Correlations 41
8.2. CFD Approaches 42
8.2.1. CFD Assessment 42

This project has received funding from the European Union's Horizon Europe research and innovation program under grant agreement No 101083558

LIST OF TABLES

*Table **1.** Comparison between experimental data (NIST) and the PR and GERG-2008 EoS of CO_2 liquid density (kg/m^3) at the saturation pressure. 12*
*Table **2.** Data of validation case 17*
*Table **3.** Thermal properties of all geological layers for the Paris basin (France). 18*
*Table **4.** Characteristics of the well completion in France. 18*
*Table **5.** Case parameters (France). 18*
*Table **6.** Case parameters (Italy). 19*
*Table **7.** Characteristics of the well completion in Italy. 19*
*Table **8.** Estimated stratigraphic profile for salt dome case (Poland). 20*
*Table **9.** The geometry of the wellbore assumed for analysis (Poland). 20*
*Table **10.** Case parameters (Poland). 20*
*Table **11.** Summary of the exchanger's input-output parameters after 20 years of operation (PL) 25*
*Table **12.** Heat Transfer Deterioration Prediction Correlations 41*
*Table **13.** Experimental Testcase Main Features 42*

LIST OF FIGURES

*Figure **1.** Comparison of density and viscosity of CO_2 calculated with the PR EoS against experimental data (NIST). 12*
*Figure **2.** Comparison of density and viscosity of CO_2 calculated with the GERG-2008 EoS against experimental data (NIST) 13*
*Figure **3.** 20-year evolution of the outlet temperature (left) and pressure drop (right) for a closed-loop with CO_2 using GERG-2008 and PR EoS. 14*
*Figure **4.** EoS impact on evolution of Pressure, Temperature diagram along the well at four times (solid lines: GERG-2008, dashed lines: Peng-Robinson) 14*
*Figure **5.** EoS impact on evolution of (a) density, (b) viscosity, (c) thermal conductivity, (d) heat capacity and (e) enthalpy along the well at four times (solid lines: GERG-2008, dashed lines: Peng-Robinson). 15*
*Figure **6.** Model validation 21*
*Figure **7.** Temporal evolution of well outlet temperature (left) and gross thermal power production (right) using water (blue line) and CO_2 (FR) 22*
*Figure **8.** Pressure-temperature profiles in the annular section (solid lines) and central tube (dashed lines) after 1 month (left) and 10 years (right) of operation for water (blue line) and CO_2 (FR) 22*
*Figure **9.** On the left: Predicted outlet temperature and well pressure increase after 10 years of continuous operation . On the right: Predicted thermal power for the first 10 years of continuous operation. Blue lines refer to water-based scenarios, while the other colors refer to CO_2-based ones. (IT) 23*
*Figure **10.** On the left: Predicted thermal power output after 10 years. Solid lines: gross thermal power output; dashed lines: specific power output (MW per km drilled). On the right: Temperature profile inside the well after 10 years of continuous operation. Blue lines refer to water-based scenarios, while the other colors refer to CO2-based ones. (IT)) 23*
*Figure **11.** Changes in output temperature (top left), power (top right) and pressure (bottom) over time (PL).*

This project has received funding from the European Union's Horizon Europe research and innovation program under grant agreement No 101083558

.....24
*Figure **12.** Temperature distribution: PL, case 2 – on the left; PL, case 3 – on the right.:* 25
*Figure **13.** - Scheme of the UNIFI approach for modelling mixtures* 32
*Figure **14.** - Possible methods for modelling mixtures* 34
*Figure **15.** Physical property variation of sCO2 as a function of temperature and pressure [40]*.....38
*Figure **16.** Temperature distribution along a non-dimensional axial coordinate (z_h = length, D = diameter) of a pipe in different heat transfer regimes for sCO_2. Solid line for bulk temperature, dashed line for wall temperature [26]* 39
*Figure **17.** Numerical domain and boundary conditions* 43
*Figure **18.** Lookup Table Sensitivity Analysis* 44
*Figure **19.** Preliminary CFD Assessment* 44

This project has received funding from the European Union's Horizon Europe research and innovation program under grant agreement No 101083558

LIST OF ABBREVIATIONS

ACRONYM	DESCRIPTION
BIP	Binary Interaction Parameter
CFD	Computational Fluid Dynamics
COSMO	Conductor-like Screening Model
EoS	Equation of State
PR	Peng-Robinson
sCO2	Supercritical Carbon Dioxide
VLE	Vapour-Liquid Equilibrium

NOMENCLATURE

SYMBOL	DESCRIPTION
A	Cross-sectional Area
c_p	Specific Heat
D	Depth
G	Mass Velocity
g	Gravity Acceleration
h	Enthalpy
L	Length
l	Axial Coordinate
m	Mass
$\dot{m}$	Mass Flow Rate
Nu	Nusselt Number
Pr	Prandtl Number
p	Pressure
q	Heat Power
T	Temperature
t	Time
w	Mass Fraction
θ	Circumferential Coordinate
ρ	Density
Φ	Volume Fraction

This project has received funding from the European Union's Horizon Europe research and innovation program under grant agreement No 101083558

EXECUTIVE SUMMARY

Scope of the deliverable

Within the framework of the HOCLOOP project, Work Package 3 addresses the investigation of alternative working fluids—specifically CO_2 and CO_2-based mixtures—as heat carriers in this innovative geothermal technology. The adoption of such fluids has the potential to improve heat transfer efficiency between the reservoir and the working fluid, thereby broadening the scope of applications beyond conventional district heating networks. To this end, the focus of this deliverable is on refining the models developed in Task 2.2 by incorporating fluid compressibility to accurately predict natural pressurisation under varying geological conditions and well configurations. In addition to a general description of the modelling approach, particular attention is devoted to a detailed analysis of key aspects related to the modelling of compressible fluids, as specified in the Grant Agreement. Finally, using the refined models, a thermodynamic comparison between water and CO_2 for some selected case studies has been carried out. The assessment of the most suitable Equation of State (Eos) for trans-critical CO_2 and CO_2-based mixtures and an analysis of heat transfer coefficients for supercritical CO_2, will be supported by specific experimental investigations planned in Task 3.1. Calibration and validation of the developed models using these experimental results will be performed in Task 3.4.

Main conclusions

The modelling of transcritical CO_2 flows in boreholes is significantly more complex than for incompressible fluids, due to the strong variability of their thermodynamic properties. A comprehensive analysis identified three key aspects to be refined in existing models: the choice of Equation of State (EoS), the formulation of governing equations for mixtures, and the definition of the heat transfer coefficient. Comparative studies revealed that discrepancies between different EoS become more pronounced at depth, while the review of literature highlighted that heat transfer can deteriorate near the pseudo-critical curve, with available correlations often being case-dependent. To address these challenges, the project partners refined their numerical tools, including the UNIFI BHEModel2.0, which allows for flexible treatment of mixture behaviour and transport equations.

These improved models were applied to three case studies: Paris (France), Gavorrano (Italy), and Goleniow (Poland). The results showed that the French site, with its low geothermal gradient, offers limited potential, with water outperforming CO_2 in terms of thermal output. The Italian site proved more promising with alternative fluids, as higher gradients allow for natural circulation and outlet temperatures of up to 110 °C, although flow rates significantly affect power output. For the Polish site, CO_2 showed lower thermal but higher electrical power output compared to water, suggesting the potential for self-sufficient systems capable of supplying both heat and electricity. Further refinements will be made once experimental results from Task 3.1 provide a validated correlation for the heat transfer coefficient.

This project has received funding from the European Union's Horizon Europe research and innovation program under grant agreement No 101083558

1. Introduction

1.1. General Introduction to WP3

Within the scope of the HOCLOOP project, WP3 focuses on investigating the use of alternative working fluids—specifically CO_2 and CO_2-based mixtures—as heat carriers in this novel geothermal technology. The type of geothermal well developed in the HOCLOOP project is indeed particularly well-suited for testing such fluids, due to the minimal interaction between the working fluid and the subsurface environment. The adoption of alternative fluids can significantly enhance heat transfer efficiency with the reservoir, potentially expanding the range of applications beyond traditional district heating networks. The main advantage of using CO_2 in place of water lies in the expected generation of a significant *thermosyphon effect* or *natural pressurization*, driven by the fluid's density variation within the well at high depth. This phenomenon leads to a higher pressure at the well outlet compared to the inlet, enabling direct mechanical power generation via a turbine or supporting the implementation of more advanced and efficient surface plant configurations for heat production or combined heat and power generation.

1.2. Objective and structure of this deliverable

This deliverable contributes to Work Package *Objective O3.2*:

> *Modelling the heat transfer, natural circulation, and pressurization features of CO_2 and other CO_2-based secondary fluids (SF) and ionic liquids (ILs) in the borehole and at surface.*

To this end, the focus is on **refining the models developed in Task 2.2 by incorporating fluid compressibility** to accurately predict natural pressurization under varying geological conditions and well configurations. In addition to the general model description, particular emphasis is placed on the detailed analysis of key aspects related to the modelling of compressible fluids—especially trans-critical CO_2 and CO_2-based mixtures—as outlined in the Grant Agreement.

- **Assessment of the most suitable Equations of State** (EoS) for modelling flows of sCO_2 (supercritical CO_2) and its smart mixtures
- **Analysis of heat transfer coefficients** between the fluid and the wellbore wall in the trans-critical region, where heat transfer performance typically deteriorates. This will be conducted through Computational Fluid Dynamics (CFD) simulations and supported by existing literature correlations.

The aspects mentioned above will be supported by specific experimental investigations planned in Task 3.1. Calibration and validation of the developed models using these experimental results will be carried out in Task 3.4.

Finally, using the refined models, a thermodynamic comparison between water and CO_2 for some selected case studies has been carried out.

Three different sites are considered in this study, representing a range of geological and thermal conditions: low-temperature silico-clastic reservoirs in France, medium- to high-temperature metamorphic reservoirs in Italy, and salt structures in Poland [1]. The utilisation of the extracted heat varies by location, reflecting the specific socio-economic context of each installation. In France and Poland, the heat is used for district

This project has received funding from the European Union's Horizon Europe research and innovation program under grant agreement No 101083558

heating, while in Italy it supports cogeneration, providing both electricity and thermal energy for greenhouse operations.

2. Analysis of Key Aspects

Due to the extreme variability of its thermodynamic properties, the modelling of transcritical CO_2 flows and their mixtures is inherently more complex than that of an incompressible fluid. Building on the models developed by the various project partners within Task 2.2, which were designed to describe the behaviour of incompressible fluids inside the borehole, a refinement is therefore required to adequately capture the peculiarities of these fluids.

A detailed analysis has been conducted to identify the fundamental aspects that must be incorporated into the model, as well as to assess how these aspects have been addressed thus far in the scientific literature. Specifically, the key aspects emerging from this analysis are:

- the selection of the Equation of State (EoS)
- the formulation of the governing equations for mixture modelling
- the definition of the heat transfer coefficient of the fluid.

To improve the readability of this document, only the assessment of EoS for single-component fluids is reported in this chapter, as these equations have already been successfully implemented in all the numerical tools. The analyses conducted on the mixture modelling and on the heat transfer coefficient (reported in Annex I and Annex II, respectively) highlighted the need for calibration with experimental data. Therefore, these aspects will be implemented in the numerical tools in Task 3.4, when the experimental results of Task 3.1 will be available.

2.1. Assessment of EoS for single component (pure) fluids

The choice of the most accurate EoS and the corresponding equations for calculating the transport (thermodynamic) properties (i.e., density, viscosity, thermal conductivity) is very important for systems in which pressure losses and heat transfer mechanisms are crucial, particularly for fluids with a narrow phase envelope, as in the case of CO_2. Here, the Peng-Robinson (PR) and the GERG-2008, two EoS commonly used in the literature, are compared against experimental data. Both equations are available in the thermodynamic tool (Carnot [2]) integrated in the flow simulator GWellFM of IFPEN.

In Table 1, the densities of the liquid phase of CO_2 at the saturation pressures for different temperatures of the PR and the GERG-2008 are compared against available experimental data (from NIST). The GERG-2008 always gives better results when compared to PR results, except for the case at the critical point. In addition, in some cases, the PR EoS failed to predict a liquid phase.

Then, the evolution of CO_2 density and viscosity for different pressures and temperatures for the PR and the GERG-2008 is compared again with experimental data in Figure **1** and Figure **2**, respectively. The GERG-2008 is far more precise in the entire range of the tested parameters.

This project has received funding from the European Union's Horizon Europe research and innovation program under grant agreement No 101083558

*Table **1.** Comparison between experimental data (NIST) and the PR and GERG-2008 EoS of CO_2 liquid density (kg/m^3) at the saturation pressure.*

T (°C)	Psat (bar)	Data	PR (Carnot)	GERG-2008 (Carnot)	PR Diff (%)	GERG Diff (%)
-56.57	5.18	1180.673	1101.066	1178.693	6.743	0.168
-51.96	6.30	1163.625	1098.478	1161.927	5.599	0.146
-47.35	7.59	1146.152	1094.679	1144.785	4.491	0.119
-42.73	9.08	1128.214	1089.520	1127.180	3.430	0.092
-38.12	10.77	1109.762	1082.876	1109.132	2.423	0.057
-33.51	12.67	1090.740	1074.570	1090.536	1.483	0.019
-28.90	14.82	1071.080	1064.410	1071.312	0.623	-0.022
-24.29	17.22	1050.701	1052.183	1051.364	-0.141	-0.063
-19.67	19.90	1029.503	1037.602	1030.525	-0.787	-0.099
-15.06	22.87	1007.362	1020.450	1008.747	-1.299	-0.137
-10.45	26.15	984.119	1000.356	985.800	-1.650	-0.171
-5.84	29.76	959.570	976.912	961.450	-1.807	-0.196
-1.22	33.72	933.436	949.539	935.324	-1.725	-0.202
3.39	38.07	905.331	917.731	907.126	-1.370	-0.198
8.00	42.82	874.688	880.559	876.199	-0.671	-0.173
12.61	48.01	840.617	-	841.631	-	-0.121
17.22	53.66	801.571	-	801.885	-	-0.039
21.84	59.82	754.418	-	753.686	-	0.097
26.45	66.53	690.565	-	688.741	-	0.264
31.06	73.84	464.743	456.207	513.525	1.837	-10.497

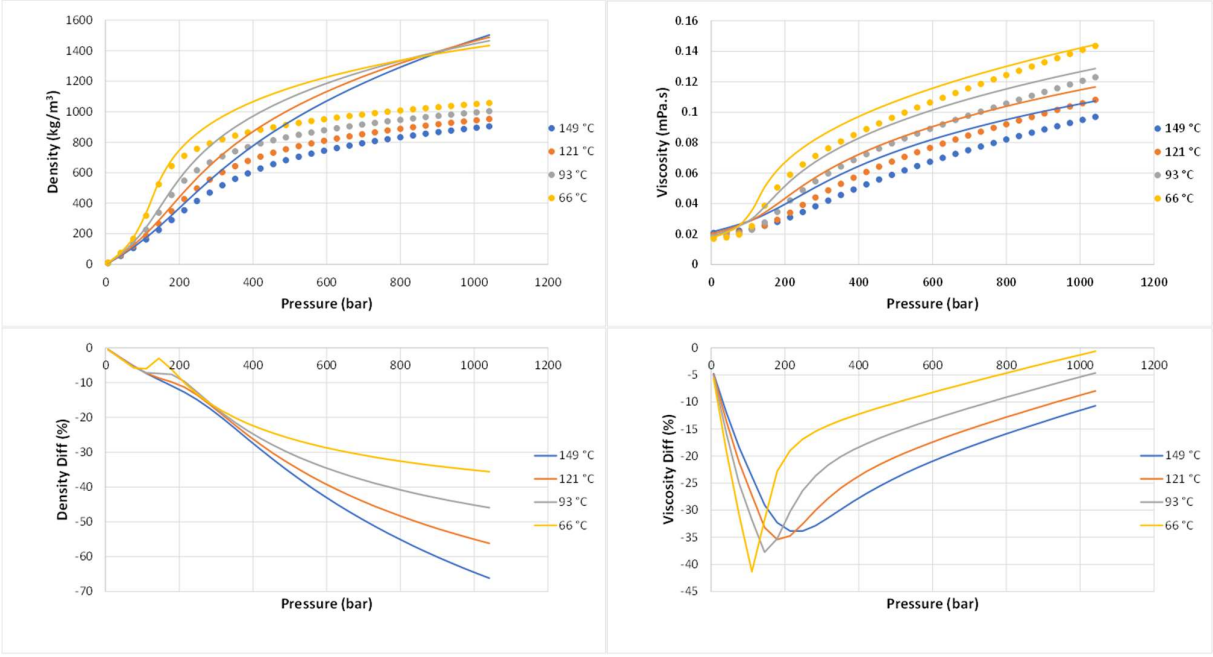

*Figure **1.** Comparison of density and viscosity of CO_2 calculated with the PR EoS against experimental data (NIST).*

This project has received funding from the European Union's Horizon Europe research and innovation program under grant agreement No 101083558

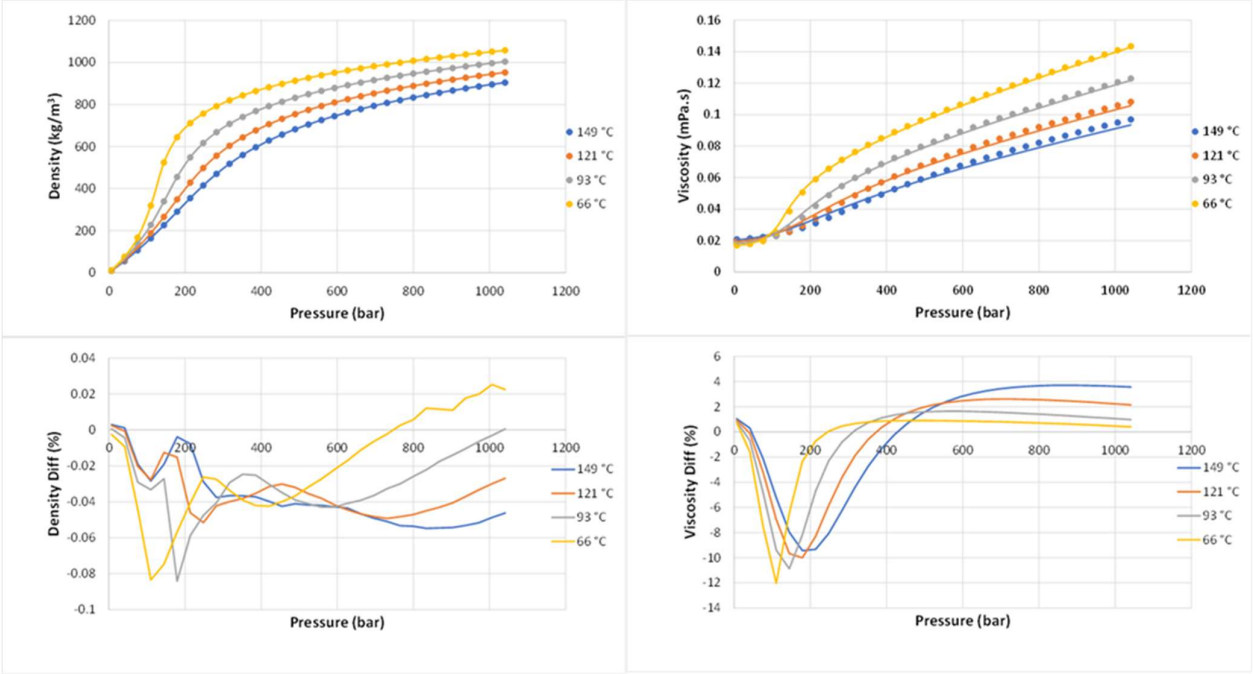

Figure 2. Comparison of density and viscosity of CO_2 calculated with the GERG-2008 EoS against experimental data (NIST).

To assess the impact of the CO_2 EoS on well flow simulator results, the PR and the GERG-2008 are compared through a well case simulated with the well flow simulator GWellFM. The Paris basin and the geometry of the existing vertical wellbore are used for the sake of comparison (summarized in Section 3.2.2). Simulations are performed with a flow rate of 5 kg/s, an inlet pressure of 100 bar and an inlet temperature of 20°C.

The simulation of the flow in the well using both EoS leads to the same temperature and pressure evolutions: a decrease that reflects the cooling of the surrounding rock and the associated heat transfer to the fluid, which also decreases. Furthermore, the discrepancies between these parameters for the two EoS simulations remain minimal, with a temperature difference of approximately 1°C (Figure **3**) and a pressure loss difference of about 2 bar (Figure **3**) over 20 years of operation. Consequently, the phase (Pressure-Temperature) diagram in Figure **4** also indicates similar behaviour, particularly at the well's entrance and exit. More significant mismatches are observed downhole, where pressure and temperature are more important.

This project has received funding from the European Union's Horizon Europe research and innovation program under grant agreement No 101083558

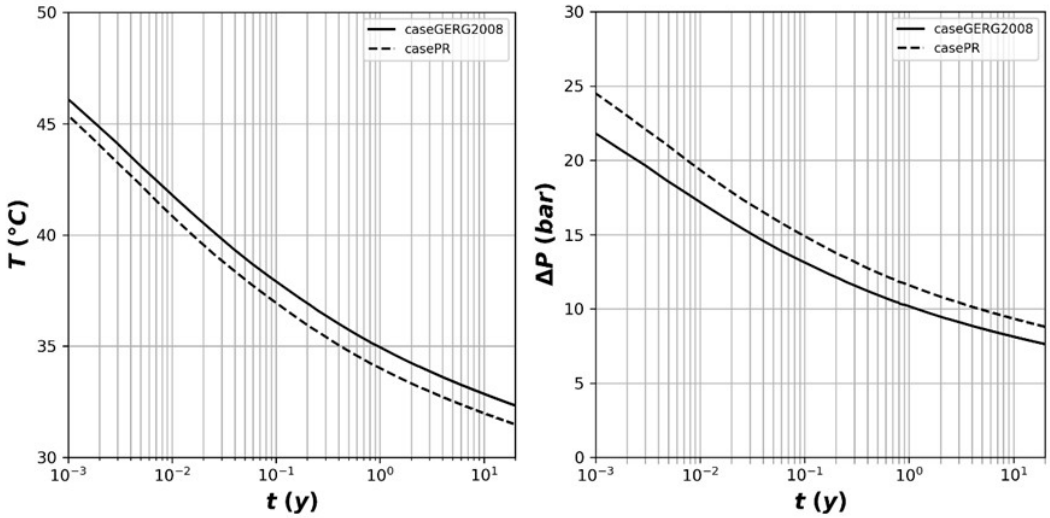

*Figure **3.** 20-year evolution of the outlet temperature (left) and pressure drop (right) for a closed-loop with CO_2 using GERG-2008 and PR EoS.*

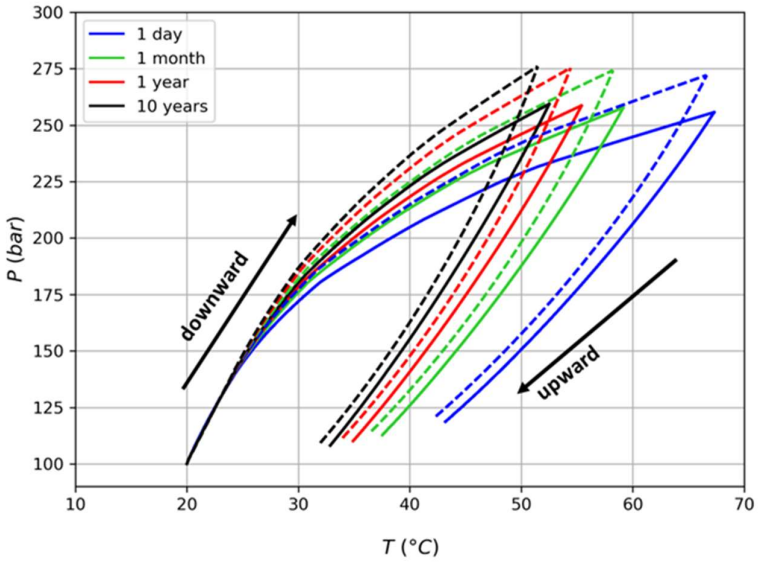

*Figure **4.** EoS impact on evolution of Pressure, Temperature diagram along the well at four times (solid lines: GERG-2008, dashed lines: Peng-Robinson).*

These properties are crucial for understanding the flow behaviour: both simulations capture the thermosiphon effect, which arises from the lower density of CO_2 in the upstream flow. This reduction in density decreases friction and pressure loss, resulting in an exit pressure higher than the entrance pressure.

Looking more closely at the evolution of density, viscosity, thermal conductivity, heat capacity, and enthalpy along the well at four different times (Figure **5**), all fluid properties show similar trends along the well, although the absolute values differ significantly between the two EoS. The maximum differences occur downhole, leading, for example, to completely distinct enthalpy values. However, the enthalpy difference between the entrance and exit, reflecting the gross energy, exhibits only minor variations.

This project has received funding from the European Union's Horizon Europe research and innovation program under grant agreement No 101083558

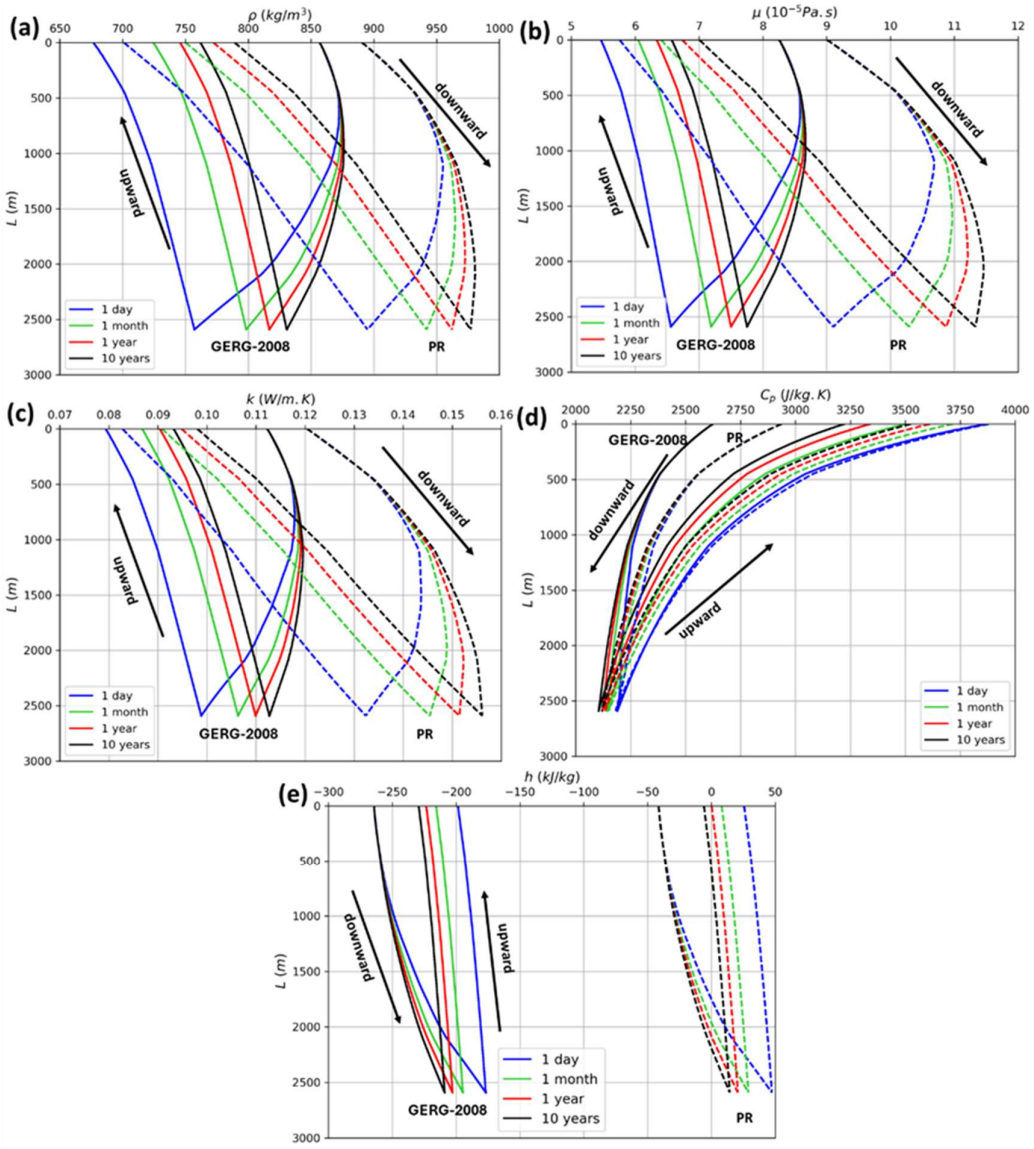

Figure 5. EoS impact on evolution of (a) density, (b) viscosity, (c) thermal conductivity, (d) heat capacity and (e) enthalpy along the well at four times (solid lines: GERG-2008, dashed lines: Peng-Robinson).

Summarising, the results of this analysis show that generally GERG-2008 appears to be the optimal EoS for modelling supercritical CO_2, as the discrepancies with experimental results are reduced in a wide range of thermodynamic conditions. This EoS is the one that is generally implemented in databases like Coolprop or Refprop. However, the discrepancies obtained using the selected EoS (PR and GERG-2008) in these geothermal systems are relevant only downhole, while they are almost negligible for the surface parameters. Consequently, both equations of state can be used when the primary focus is on the surface parameters estimation (i.e. coupling with surface installation).

This project has received funding from the European Union's Horizon Europe research and innovation program under grant agreement No 101083558

3. Methodology

3.1. Developed Numerical Tools for Compressible Fluids

Each partner has refined its own numerical tool, each characterized by specific assumptions and modelling approaches. These tools have been compared and benchmarked to assess the impact of the underlying assumptions, following a methodology like that adopted in Task 2.2. The developed tools include: **GWellFM** (IFPEN), **BHEModel2.0** (UNIFI), and **GTW** (IFE).

All tools:

- are 1D and axisymmetric
- are semi-transient geothermal simulators in cylinder coordinates, solving the equation for transient heat conduction for cooling or heating of the rock, assuming, however, stationary advective (by the fluid) and convective heat transport in the wellbore
- solve the momentum, energy and mass balances
- calculate the heat losses due to conduction and forced convection, as well as pressure losses due to friction and gravity.

The impact of using CO_2 instead of water [3] in closed-coaxial wells extended by a horizontal section is studied, with the fluid being injected into the annular space, while it returns to the surface through the central tube.

3.1.1. BHEModel2.0 (UNIFI)

BHEModel2.0 is based on the numerical integration of equations (1) and (2) - *see section 2* - along the well using a Runge-Kutta scheme [4]. The heat transfer between the well and the surrounding rocks has been evaluated using a well-known correlation, which has been extended to account for the possible presence of a convective fluid in a reservoir around the well. A time convolution approach has been implemented for extending the correlation to cases with variable extraction rates as originally proposed by [5]. The fluid properties and derivatives are directly retrieved with REFPROP [6].

3.1.2. GWellFM (IFPEN)

GWellFM (Geothermal Well Flow Model) considers the single-phase flows of liquids and gases, the hydrodynamics of the two-phase downward and upward flows, constitutive laws for mixtures, and the heat transfer between the well completion and the surrounding formation [7]. The model is fully compositional and, to perform the thermodynamic calculations, a thermodynamic engine has been integrated into the code [2]. The calculations are performed in thermodynamic equilibrium and several Equation-of-States are available (Cubic-Plus-Association, Peng-Robinson, GERG-2008, Kestin and others). The energy balance is solved based on enthalpy (Pressure-Enthalpy tracking) for more precise calculations when it comes to fluids like CO_2.

3.1.3. GTW (IFE)

GTW (Geo-Thermal-Well) is a single-phase and semi-transient geothermal simulator in cylinder coordinates [8]. It is the coupling of a 1D pipe-flow solver with an implicit and transient temperature solver for the well flow and the rock. These two models are serially coupled, with the temperature solution from the cell-centred FVM (finite-volume method) model providing the 1D pipe model with the surrounding heat

This project has received funding from the European Union's Horizon Europe research and innovation program under grant agreement No 101083558

flow. In return, a solution from the 1D pipe model provides the FVM model with fluid properties for the pipe cells in the mesh. Two or three global iterations are normally sufficient for convergence for the pressure and temperature solutions. The FVM temperature solver applies an implicit formulation of the energy balance to simulate the transient cooling of the rock. The pipe simulator solves the equations for stationary mass-flow, momentum and energy conservation of the fluid. The fluid properties such as heat capacity, enthalpy, viscosity etc. are taken from tables of pressure and temperature.

3.2. Case studies

3.2.1. Model validation

GWellFM and GTW have been recently benchmarked against analytical solutions for the case of water circulation in a deep coaxial closed heat exchanger [9, 10]. Here, the same case (Table **2**) of a closed coaxial L-shaped well with CO_2 being injected in the annular space is run with the three HOCLOOP case studies.

*Table **2.** Data of validation case*

	Variable	Unit	Value
Wellbore	Depth, *D*	m	4500
	Hor. Length, *L*	m	2000
Inner tubing	Inner diam., *ID*	cm	9.715
	Thickness, *h*	cm	2.312
	Roughness, ε	mm	0.045
	Conductivity, *k*	W/m/K	0.01
Casing	Inner diam., *ID*	Cm	27.939
	Thickness, *h*	Cm	0.856
	Roughness, ε	mm	0.045
	Conductivity, *k*	W/m/K	45
Rocks	Conductivity, *k*	W/m/K	2.423
	Density, ρ	kg/m^3	2360
	Capacity, C_p	J/kg/K	930
Inlet conditions	Temperature, T_{in}	°C	10
	Pressure, P_{in}	bar	50
	Flow rate, *m*	kg/s	5
Boundary conditions	Surface temp., T_{surf}	°C	20
	Gradient, g_T	°C/m	0.04

3.2.2. France

The Parisian basin subsurface is exploited by deep geothermal doublets for district heating since 1969 and the density of the exploitation of the Dogger carbonates is the largest in the world with 50 doublets in activity. New reservoirs are targeted as the deeper and hotter Trias (up to 90 °C) or the shallower and more accessible lower cretaceous (35-40°C), both silico-clastic reservoirs. However, the Trias projects realised in the 1980's have failed due to a rapid loss of injectivity, and the lower Cretaceous of recent realizations face similar difficulties. To reach the target of the French pluri-annual energy plan, different options must be considered, among which the HOCLOOP concept. The geological setting of this case study is representative of a sedimentary basin in thermal equilibrium and thus with a normal geothermal gradient.

This project has received funding from the European Union's Horizon Europe research and innovation program under grant agreement No 101083558

Table **3** and Table **4** summarize the properties of the geological setting of the Paris basin and the geometry of the existing wellbore. Water and CO_2 as heat transfer fluids with different flow rates and different horizontal lengths are considered, according to Table **5**

*Table **3**. Thermal properties of all geological layers for the Paris basin (France).*

Layer	Bottom [m MD]	Temperature [°C]	Conductivity [W/m/K]	Heat Capacity [J/(kg K)]	Density [kg/m³]
Surface	0	15	-	-	-
Albian	548	30.6	1.59	903	2380
Gault shale	608	32.6	3.16	859	2270
Barremian	754	38.3	1.63	915	2480
Oxfordian	1322	58.4	2.24	795	2390
Callovian	1623	68.1	1.73	917	2590
Lower Callovian	1727	71.7	2.14	805	2450
Bathonian	1767	73.7	2.14	806	2590
Dommerian	1963	81.0	1.74	915	2600
Rhetian	2146	88.0	2.63	887	2510
Anisian	2590	100.4	2.94	710	2370

*Table **4**. Characteristics of the well completion in France.*

Segment	Top [m MD]	Bottom [m MD]	Slope [°]	Drilling [mm]	Casing ID [mm]
1	0	450	90	660.4	309.245
2	450	1100	50	431.8	198.755
3	1100	2090	49	304.8	198.755
4	2090	2276	49	215.9	198.755
5	2276	2590	49	215.9	198.755
6	2590	4590	0	194	175

*Table **5**. Case parameters (France).*

	Fluid	L (km)	m [kg/s]	T_{in} [°C]	P_{in} [bar]
Case 1	Water	2	3	25	6
Case 2	CO_2	1	3	20	100
Case 3	CO_2	2	3	20	100
Case 4	CO_2	2	10	20	100
Case 5	CO_2	2	3	20	120
Case 6	CO_2	2	3	30	100

This project has received funding from the European Union's Horizon Europe research and innovation program under grant agreement No 101083558

3.2.3. Italy

Among the three Italian case studies analysed in the scope of the HOCLOOP project, the most interesting one from a scientific perspective is Gavorrano. Gavorrano is a small village near the southern coast of Tuscany. It has originally attracted geologists' attention because of the presence of a pyrite mine and some abandoned quarries that allow a detailed reconstruction of the geological setting of the area [11]. It is roughly located between the traditional Larderello and Amiata geothermal areas. Despite being relatively far from both, the geothermal gradient in the Gavorrano area is expected to be higher than 50°C/km [12], which makes it an appealing candidate for a possible closed-loop application. The surrounding area has a significant heating demand due to the presence of multiple villages and small towns, potentially interested in developing a geothermal-powered district heating network [13]. Three well geometries have been analysed in this case study (Table 6). The first two correspond to the economic optima for CO_2 and water, respectively, as identified by [13] using a simplified well model. Since the optimal geometries differ for CO_2 and water, a third case has been added to enable a direct comparison: CO_2 circulation in a well with the same geometry as the water-optimized configuration. Well diameters and slopes are the same as described in Table 7 for all three cases. The well modelling is simplified because the presented analysis is a preliminary evaluation. The inlet pressure and temperature were kept constant for both water (10°C, 6 bar) and CO_2 (10°C, saturated liquid conditions), while multiple flow rates were tested for each case. The range of CO_2 flow rates is higher than that of water, due to its lower specific heat.

Table 6. Case parameters (Italy).

	Fluid	Depth (km)	L (km)	*m* [kg/s]
Case 1	Water	4.25	3.75	5 - 15
Case 2	CO_2	3.25	2.375	10 - 25
Case 3	CO_2	4.25	3.375	10 - 30

Table 7. Characteristics of the well completion in Italy.

Segment	Slope [°]	Drilling [mm]	Casing ID [mm]	Tubing OD [mm]	Tubing ID [mm]
1 (Vertical)	90	508	279.4	143	97
2 (Horizontal)	0	381	279.4	143	97

3.2.4. Poland

The case study in Poland evaluates salt structures, the Goleniów salt dome, as potential targets for applying the closed-loop technology developed in the HOCLOOP project. These structures are typically found in sedimentary basins, where extensive salt deposits have formed and are among the best geologically recognized forms. The northern Goleniów salt dome along the direction NNW-SSE has dimensions of 4.5 × 2.0 km. One exploration well has been drilled in the area. It reaches a depth of 3649 m and was drilled through the evaporite series of Zechstein from 888 m depth to 3649 m, reaching a thickness of >2761 m. The temperature profiling was performed in the depth interval up to 2800 m, where

This project has received funding from the European Union's Horizon Europe research and innovation program under grant agreement No 101083558

the temperature was measured at approximately 99°C. It is worth remarking that the measurements were taken in unstable thermal conditions and in the lower part of the profile the temperature disturbance which required correction is noticeable. The average geothermal gradient for Permian formations (salt dome) is at 2.5°C/100 m, while in the zone above the salt dome the geothermal gradient for Mesozoic formations is about 3.5°C/100 m. The average geothermal gradient for the entire profile in this area is about 3°C/100 m. Tables **8** and **9** summarize the properties of the geological setting and the geometry of the wellbore assumed for analysis, while

Table **10** shows the basic operating parameters of the HOCLOOP system adopted in each case.

*Table **8.** Estimated stratigraphic profile for salt dome case (Poland).*

Depth [m]	Stratigraphy	Temperature [°C]
0	Quaternary	10
35	Tertiary	20
439	Cretaceous	40
657.6	Upper Jurassic	47
702.2	Permian	48
4300	Permian	126

*Table **9.** The geometry of the wellbore assumed for analysis (Poland).*

L [m MD]	ID [mm]	Slope [°]
0 - 900	450.977	90
900 - 3690	313.6138	90
3690 - 4500	313.6138	34.931
4500 - 7000	216.789	0

*Table **10.** Case parameters (Poland).*

	Fluid	m [kg/s]	T_{in} [°C]	P_{in} [bar]
Case 1	Water	5.556	35	6.1
Case 2	CO_2	10	35	140
Case 3	CO_2	15	35	140

This project has received funding from the European Union's Horizon Europe research and innovation program under grant agreement No 101083558

4. Results

4.1. Model validation

The three models show a similar behaviour, predicting very close values of the outlet temperature (Figure 6a) and pressure (Figure 6b). The discrepancies between the three codes are mainly attributable to the difference in the energy balance, the solution of the transient problem and the fluid's properties calculator. GWellFM considers the enthalpy of the fluid, whereas GTW and BHEModel solves the energy balance based on the temperature with extra terms for the thermal expansibility and compressibility. On the other hand, both GWellFM and GTW numerically solve the unsteady and 2D heat transfer expressed by the radial Fourier heat conduction equation, whereas BHEModel considers an analytical solution based on a time function. Another source of discrepancy of the different simulators comes from the use slightly different data for CO_2. A slight difference in density as a function of pressure and temperature leads to different fluid pressure. The same applies to the enthalpy, the heat capacity, the fluid compressibility, and the thermal expansibility. A slight difference in these properties as a function of pressure and temperature may lead to slightly different results.

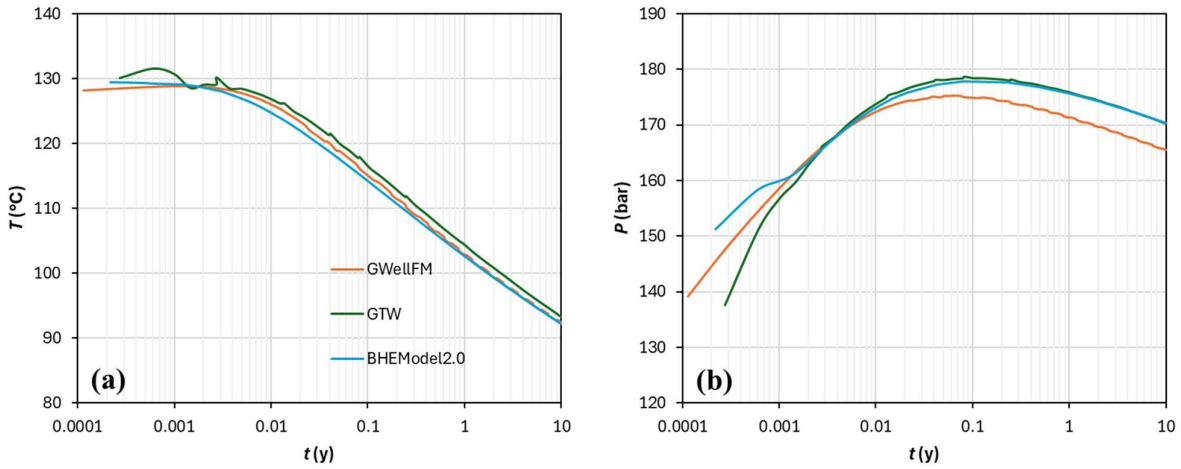

Figure 6. Model validation.

4.2. French Case Study

The gross thermal power of the borehole heat exchanger is defined as the product of the mass flow rate of the circulating fluid and the enthalpy difference between outlet and inlet.

Figure 7 shows the time evolution of the fluid's temperature at the outlet of the return tube and the power production, respectively. In all cases, there is a rapid decrease in temperature and in the corresponding energy production due to the highly transient nature of the heat transfer mechanism. For water (blue line), this effect is more pronounced because it recovers more energy, resulting in faster cooling of the surrounding rocks. However, the water proved to be the optimal case, since the temperature of the fluid is several degrees higher than that of CO_2.

This project has received funding from the European Union's Horizon Europe research and innovation program under grant agreement No 101083558

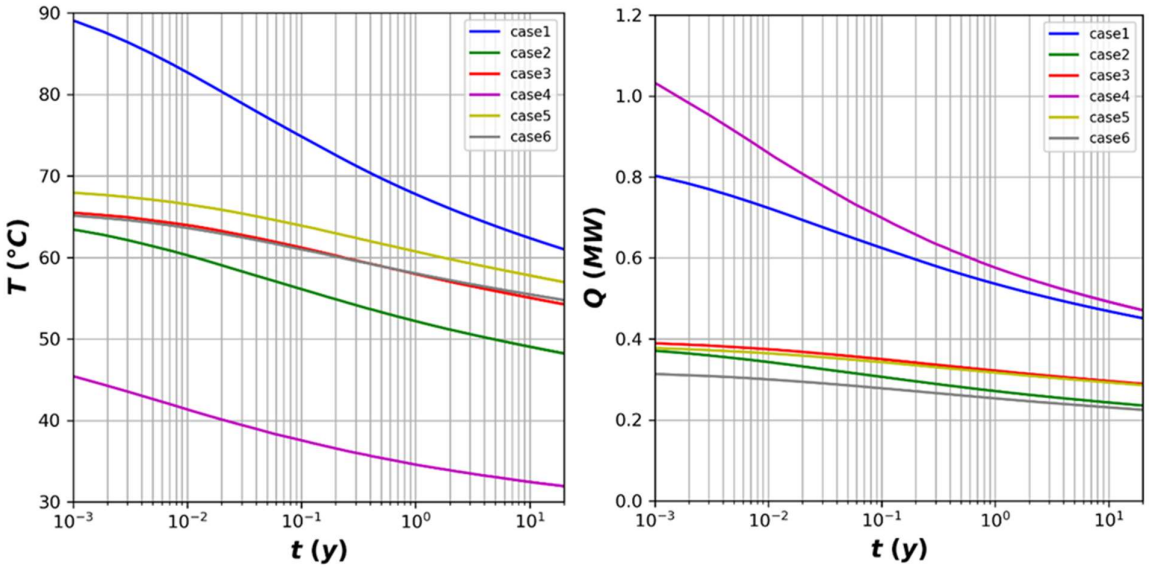

Figure 7. Temporal evolution of well outlet temperature (left) and gross thermal power production (right) using water (blue line) and CO_2 (FR)

The CO_2 has a higher energy output only in the case of a higher flow rate, because the produced energy depends linearly on the flow rate. For the same case, the output temperature is the worst, because the fluid moves faster in the well, resulting in lower residence time, thus, in lower heat recovery. In addition, the pressure losses due to the higher velocity are higher. It can be observed in Figure 8, where the profiles of pressure and temperature along the well are traced. Except for Case 4, in all the other cases with CO_2, the output pressure is higher than the injection pressure, which is caused by the thermosiphon effect and the impact of the decrease in fluid density while travelling from the inlet to the outlet of the closed-loop well. Only at a higher flow rate (Case 4), the outlet pressure is lower, because of the higher losses due to the friction. The pressure difference between outlet and inlet is higher for the lower flow rate, the lower injection temperature and the longer horizontal section.

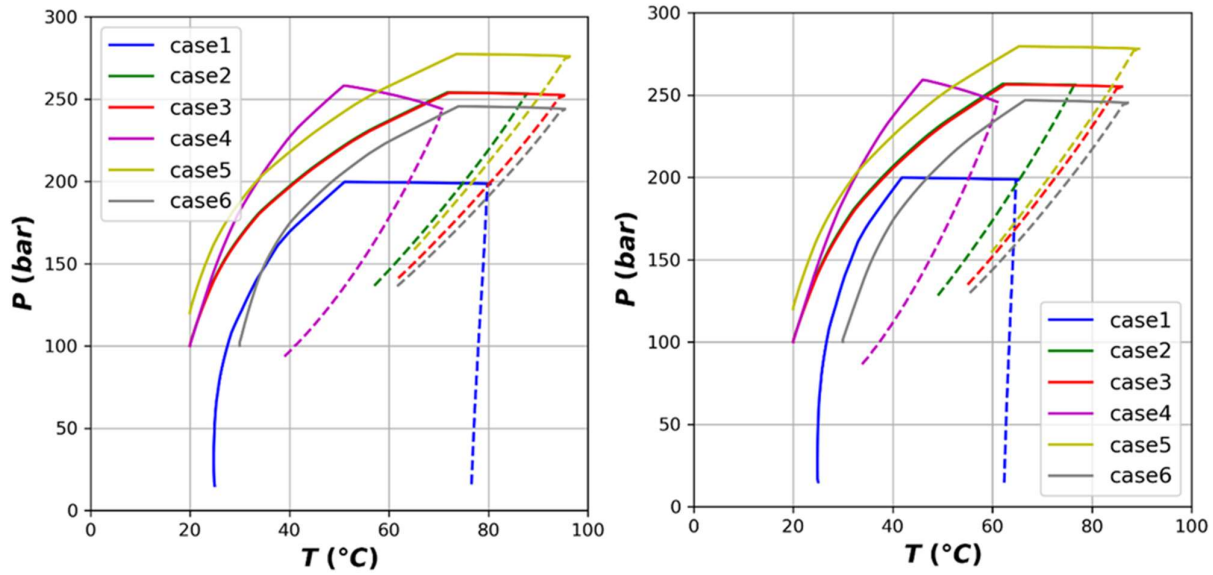

Figure 8. Pressure-temperature profiles in the annular section (solid lines) and central tube (dashed lines) after 1 month (left) and 10 years (right) of operation for water (blue line) and CO_2 (FR)

This project has received funding from the European Union's Horizon Europe research and innovation program under grant agreement No 101083558

4.3. Italian case study

Due to the increased geothermal gradient and well length compared to the Paris case, the power extraction is expected to be much higher for the Italian case, as shown in Figure **9**. In particular, the water-based configuration (Case 1) is projected to extract more than 3 MW after 10 years of operation. The CO_2-based configurations yield slightly lower outputs: approximately 2.5 MW for the well with the same geometry as the water case (Case 3) and about 1.5 MW for the CO_2-optimized geometry (Case 2).

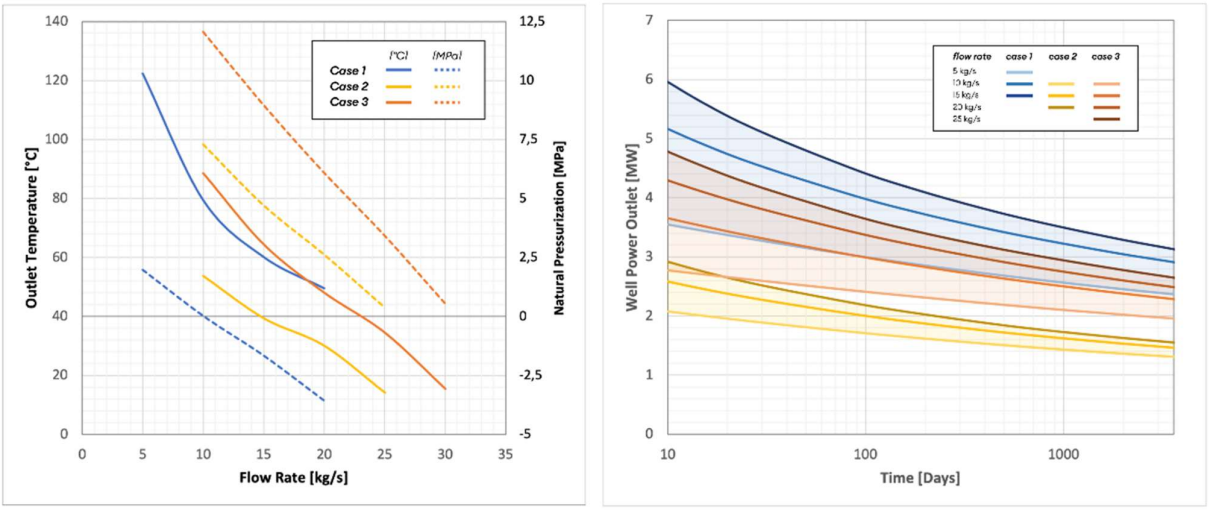

*Figure **9.** On the left: Predicted outlet temperature and well pressure increase after 10 years of continuous operation . On the right: Predicted thermal power for the first 10 years of continuous operation. Blue lines refer to water-based scenarios, while the other colors refer to CO_2-based ones. (IT)*

In terms of outlet temperature and pressure, the water-based system is expected to deliver a higher temperature, but with limited natural pressurization. In fact, for flow rates exceeding 10 kg/s, pumping is required to maintain circulation. Conversely, CO_2 emerges from the well at a lower temperature but with significantly higher pressure, enabling natural circulation under a wider range of operating conditions.

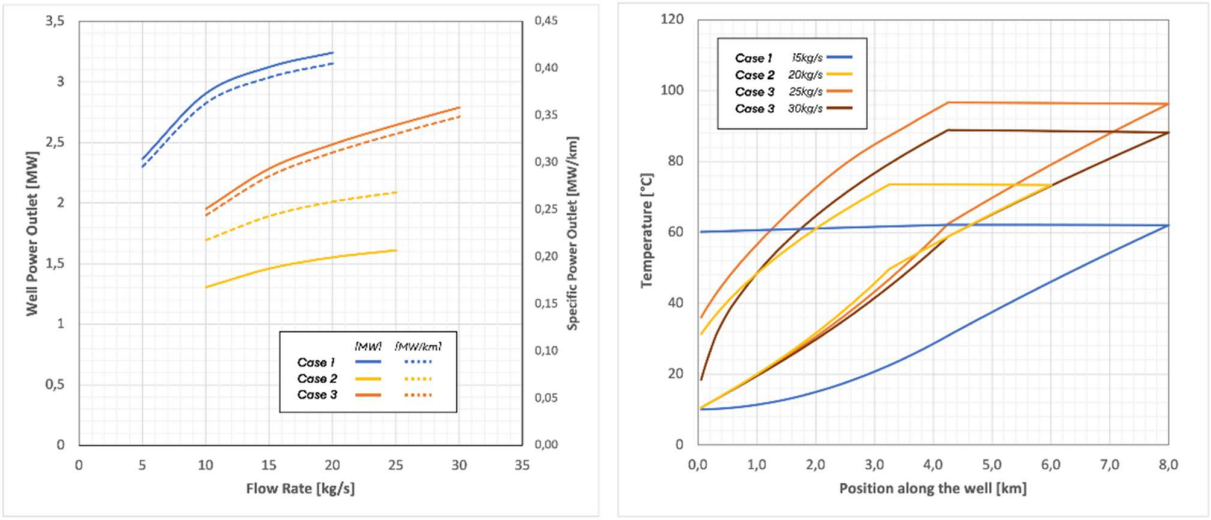

*Figure **10.** On the left: Predicted thermal power output after 10 years. Solid lines: gross thermal power output; dashed lines: specific power output (MW per km drilled). On the right: Temperature profile inside the well after 10 years of continuous operation. Blue lines refer to water-based scenarios, while the other colors refer to CO2-based ones. (IT)).*

This project has received funding from the European Union's Horizon Europe research and innovation program under grant agreement No 101083558

The lower energy output of the CO2-based configuration is primarily due to reduced heat transfer with the surrounding rock per drilled km, as shown in Figure 10. This occurs because the temperature difference between the rock and the fluid is smaller, a consequence of CO2's temperature increase with depth due to its higher compressibility (Figure 10, right).

The main advantage of the CO_2-based systems is that the energy is extracted in a more versatile form (e.g. mechanical besides thermal, due to the much larger pressurization), which can help to increase the profitability of the overall system despite the lower gross heat power output.

4.4. Polish case study

The GTW software was used to simulate the operation of the HOCLOOP technology for the selected cases. Figure **11** summarises the main results. A rapid stabilization of output parameters from the borehole heat exchanger is evident in all cases. Changes in the long term are small. It can be observed that increasing the CO_2 flow rate results in a decrease of output temperature and pressure. However, the total output power of the heat exchanger increases. In all cases, the thermosyphon effect is observed. Temperature changes with depth in the HOCLOOP heat exchanger are shown in Figure 11. Table 11 shows a summary of the heat exchanger's input-output parameters after 20 years of operation.

In the case of CO_2, the temperature in the deviated and vertical parts of the tubing significantly decreases compared to water, while in the horizontal section, it remains almost constant. This is due to changes in the properties of CO_2 as a function of temperature and pressure, as well as the Joule-Thomson effect. Throughout the system, CO_2 remains in a supercritical state.

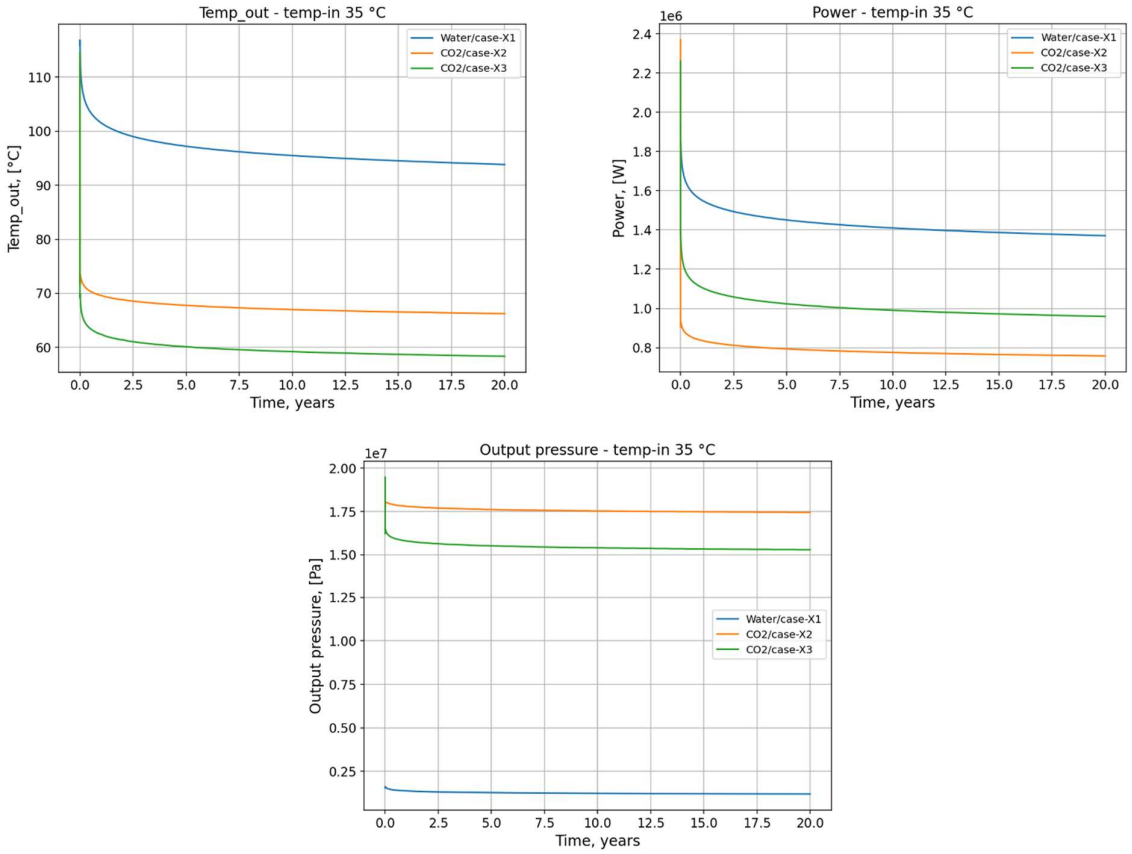

*Figure **11.** Changes in output temperature (top left), power (top right) and pressure (bottom) over time (PL).*

This project has received funding from the European Union's Horizon Europe research and innovation program under grant agreement No 101083558

Based on the data presented in Table 11, a more precise assessment of the possibilities of obtaining useful power was made.

*Table **11.** Summary of the exchanger's input-output parameters after 20 years of operation (PL)*

					Output after 20 yeas		
	Fluid	Flow rate [kg/s]	T_{in} [°C]	p_{in} [MPa]	T_{out} [°C]	p_{out} [MPa]	Electricity/heat Power share P_{el}/P_{th} [kW]
Case 1	Water	5.556	35	0.61	93.84	1.2	1 / 1 368
Case 2	CO_2	10	35	14	66.24	17.45	46 / 712
Case 3	CO_2	15	35	14	58.34	15.29	21 / 943

Since the obtained thermosyphon effect significantly exceeds the range of pressure losses in the surface installation, it is possible to use it to generate electrical power. Assuming 3 bar fluid flow resistance through the surface installation, in addition to thermal power, it is possible to generate electricity. Due to the relevant output overpressure in the case of CO_2, a significant amount of electric power can be expected. Electric power, W_{el} [W], in the case of water (case 1), is estimated as:

$$W_{el} = \frac{m(P_{out} - P_{in} - \Delta P)\eta_{wt}}{\rho} \quad (1)$$

where m is the flow rate [kg/s], P_{out} and P_{in} is output and inlet pressure [Pa], ΔP is the pressure losses in the surface energy system [Pa], ρ is the average density [kg/m^3] of water in the range of temperature and pressure between output and input and η_{wt} is the efficiency of water turbine (assumed as 0.75).

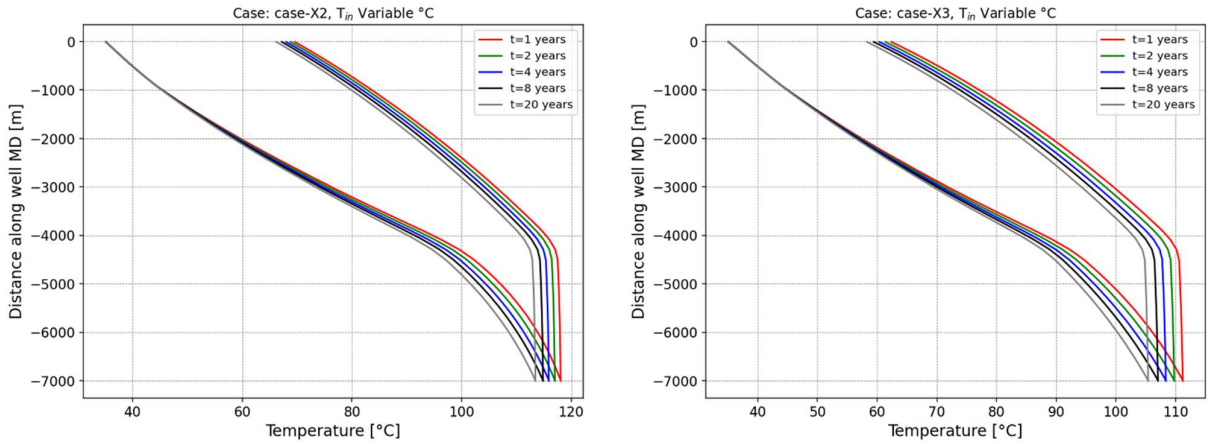

*Figure **12.** Temperature distribution: PL, case 2 – on the left; PL, case 3 – on the right.:*

The electric power output in the case of CO_2 is estimated based on the equation:

$$W_{el} = m(h_{out} - h) \quad (2)$$

where h_{out} is the enthalpy of CO_2 on output of the BHE [J/kg], h is the enthalpy of CO_2 downstream a

This project has received funding from the European Union's Horizon Europe research and innovation program under grant agreement No 101083558

supercritical CO_2 turbine [J/kg], estimated as:

$$h = h_{out} - \eta_{scCO_2}[h_{out} - h(P_{in} + \Delta P, T_{in})] \quad (3)$$

with η_{scCO2} the internal efficiency of supercritical CO_2 turbine (assumed as 0.9), $h(P_{in}+\Delta P, T_{in})$ the enthalpy [J/kg] of CO_2 in the pressure of the input to the borehole heat exchanger enlarged on pressure losses in the surface part of the installation (assumed to be equal 3 bar) and T_{in} the temperature at input to the borehole heat exchanger [K].

The thermal power of the system was estimated based on equations:

- in the case of water:

$$P_{th} = mC_p(T_{out} - T_{in}) \quad (4)$$

- in the case of CO_2:

$$P_{th} = m[h'(P_{in} + \Delta P, T_{in}) - h_{in}] \quad (5)$$

where P_{th} is the heat power of the solution [W], C_p is the mass-specific heat capacity of liquid water. The enthalpy of sCO_2, considering an adiabatic expansion of the fluid from conditions at the deep borehole heat exchanger to pressure $P_{in}+\Delta P$ and temperature T_{in} [J/kg] is an averaged value in the temperature and pressure range between T_{in}-T_{out} and P_{in}-P_{out} [J/(kg K)], $h'(P_{in}+\Delta P, T_{in})$. The value is higher on $h(P_{in}+\Delta P, T_{in})$ on internal $scCO_2$ turbine efficiency as follows:

$$\frac{h'(P_{in} + \Delta P, T_{in}) - h_{in}}{h'(P_{in} + \Delta P, T_{in}) - h_{in}} = \eta_{CO_2} \quad (6)$$

with h_{in} the enthalpy of CO_2 at input of the deep heat exchanger [J/kg],

The calculations are based on thermal properties of fluids estimated by CoolProp library ver. 6.1.1 (http://www.coolprop.org/index.html). Finally, based on the described assumptions, the output powers were estimated and presented in Table 11.

This project has received funding from the European Union's Horizon Europe research and innovation program under grant agreement No 101083558

5. Conclusions

Because of the extreme variability of their thermodynamic properties, the modelling of transcritical CO_2 flows and their mixtures is inherently more complex than that of incompressible fluids. Building on the models developed by the project partners in Task 2.2, originally designed to describe the behaviour of incompressible fluids inside the borehole, a refinement is required to adequately capture the specific characteristics of these fluids.

A detailed analysis has been conducted to identify the fundamental aspects to be incorporated into the refined model, as well as to assess the extent to which these aspects are addressed in the scientific literature. The key aspects emerging from this analysis are:

- the selection of the Equation of State (EoS).
- the formulation of the governing equations for mixture modelling.
- the definition of the heat transfer coefficient of the fluid.

A comparative analysis of EoS for CO_2 has shown that, when simulating fluid behaviour in a borehole, significant discrepancies arise at greater depths, where temperature and pressure conditions become relevant. By contrast, near the surface, these discrepancies remain limited, with pressure differences of approximately 2 bar and temperature differences of about 1 °C over 20 years of operation.

Moreover, the modifications required for mixture modelling have been presented In Annex I with reference to the model developed by UNIFI (BHEModel 2.0), highlighting that different formulations of the transport equations can be adopted depending on the degree of miscibility of the components and the level of detail required in the analysis.

Concerning the heat transfer coefficient (Annex II), the literature review has shown that, due to the variability of the thermodynamic properties of the fluid, local deteriorations in heat transfer performance can occur in the vicinity of the pseudo-critical curve. These effects, observed mainly in applications with high thermal loads, may nonetheless arise under specific geothermal gradient conditions and borehole geometries. The review has also indicated that, while empirical correlations are generally available to estimate and predict these effects, they often remain strongly case-dependent. More advanced modelling approaches (i.e., low-fidelity CFD) face the same limitation, as turbulence models fail to fully capture the complex fluid-dynamic interactions near the wall. Consequently, a specific correlation for the heat transfer coefficient will be derived using the numerical results from the experimental campaign of Task 3.1. This correlation, obtained in thermodynamic conditions that are representative of the geothermal well, will be implemented in the numerical tools to have a more accurate prediction of the total heat extracted from the well.

Following these analyses, each partner refined their own numerical tool. These models were subsequently adopted to compare the performance of different fluids (water and CO_2) in selected project case studies, specifically Paris (France), Gavorrano (Italy), and Goleniów (Poland).

The low temperature of the French site seems to suggest that it is a non-optimal candidate for the closed-loop systems, especially when compared to the conventional geothermal applications. For all tested cases, the thermal output was relatively low, and water proved to be higher performing than sCO_2. The potential

This project has received funding from the European Union's Horizon Europe research and innovation program under grant agreement No 101083558

advantage of using CO_2 for creating a natural circulation due to the thermosiphon effect was shown through the increase in the outlet pressure.

The Italian case looks much more promising, given the higher geothermal gradient. Both water and CO_2 are expected to allow for the working fluid to naturally circulate in the well (at lower flow rates with CO_2). Depending on the flow rate, the outlet temperatures can be as high as 110°C. However, they are significantly lower due to the need for a higher flow rate to obtain a significant power output.

For the Polish site, the results show that the use of CO_2 is characterised by lower heat extraction with respect to water but, conversely, higher electric power generation. In the case of water, the achievable electrical output is negligible; whereas sCO_2 is more promising in this regard. The generated electric power can be used to drive auxiliary equipment, such as pumps, thereby supporting a self-sufficient heat supply system. In addition, the extracted heat shows string potential, as it can serve as a baseload of the heat demand curve in various applications analyzed.

An additional refinement of these models will be performed once a correlation for the heat transfer coefficient is derived from the results of the experimental activities of Task 3.1.

This project has received funding from the European Union's Horizon Europe research and innovation program under grant agreement No 101083558

6. References

[1] M. Singh, C. Souque, D. Liotta, D. Fiaschi, B. Laenen, V. Harcouët-Menou, P. Wojnarowski and L. Pająk, "Pilot sites data and integration analysis D4.1_V2," HOCLOOP Project 101083558, 2024.

[2] J. de Hemptinne, N. Ferrando, M. Hajiw-Riberaud, V. Lachet, S. Maghsoodloo, P. Mougin, T. Ngo, L. Pigeon, J. Romero Yanes and A. Wender, "Carnot: a thermodynamic library for energy industries," *Science and Technology for Energy Transition,* vol. 78, p. 23, 2023.

[3] E. Hernandez, J. Pogacnik, V. Leontidis, H. Pham, P. Wojnarowski, L. Pająk, M. Kaczmarczyk, D. Fiaschi, P. Ungar, F. Gigliotti and E. Falchini, "Underground simulations of the HOCLOOP concept at the selected pilot sites," HOCLOOP Project 101083558, 2025.

[4] P. Ungar, "Use of CO2 as working fluid in geothermal systems, PhD Dissertation," Univeristy of Florence, Florence, Italy, 2024.

[5] Y. Zhang, L. Pan, K. Pruess and S. Finsterle, "A time-convolution approach for modeling heat exchange between a wellbore and surrounding formation," *Geothermics,* pp. 261-266, 2011.

[6] E. Lemmon, I. Bell, M. Huber and M. McLinde, "NIST Standard Reference Database 23: Reference Fluid Thermodynamic and Transport Properties-REFPROP, Version 10.0," National Institute of Standards and Technology, 2018.

[7] V. Leontidis, P. Niknam, I. Durgut, L. Talluri, G. Manfrida, D. Fiaschi, S. Akin and M. Gainville, "Modelling reinjection of two-phase non-condensable gases and water in geothermal wells," *Applied Thermal Engineering,* vol. 223, p. 120018, 2023.

[8] M. Wangen, "Numerical solutions for coaxial borehole heat exchangers using CO2 as a working fluid," *Applied Thermal Engineering,* vol. 264, 225.

[9] V. Leontidis, M. Wangen, P. Ungar and D. Fiaschi, "Flow pipe model for fluid circulation D2.2," HOCLOOP Project 101083558, 2023.

[10] V. Leontidis, E. Hernandez, J. Pogacnik, M. Wangen and V. Harcouët-Menou, "Controlling injection conditions of a deep coaxial closed well heat exchanger to meet irregular heat demands: a field case study in Belgium (Mol)," *Geothermal Energy,* vol. 13, p. 10, 2025.

[11] A. Brogi, A. Caggianelli, D. Liotta, M. Zucchi, A. Spina, E. Capezzuoli, A. Casini and E. Buracchi, "The Gavorrano Monzogranite (Northern Apennines): An Updated Review of Host Rock Protoliths, Thermal Metamorphism and Tectonic Setting," *Geosciences,* vol. 11, p. 124, 2021.

[12] B. Vedova, S. Bellani, G. Pellis and P. Squarci, "Deep temperatures and surface heat flow distribution," in *Anatomy of an Orogen: the Apennines and Adjacent Mediterranean Basins*, Dordrecht , Springer, 2001, pp. 65-76.

[13] D. Fiaschi, P. Ungar, F. Gigliotti and A. Meana-Fernandez, "Thermo-Economic Analysis of a Geothermal-driven District Heating Network: comparison between a water-based and a CO2-based

This project has received funding from the European Union's Horizon Europe research and innovation program under grant agreement No 101083558

grid," *Submitted to Applied Thermal Engineering,* 2025.

[14] E. W. Lemmon and R. T. Jacobsen, "A Generalized Model for the Thermodynamic Properties of Mixtures," *International Journal of Thermophysics,* vol. 30, no. 3, 1999.

[15] I. H. Bell and E. W. Lemmon, "Automatic Fitting of Binary Interaction Parameters for Multi-fluid Helmholtz-Energy-Explicit Mixture Models," *Journal of Chemical & Engineering Data,* no. 61, 2016.

[16] D. Menegazzo, G. Lombardo, L. Fedele, S. Bobbo, M. S. Kim, Y. Jeong and S. Lee, "Isothermal (vapor + liquid) equilibrium measurements and correlation of the binary mixture 3,3,3-trifluoropropene (R1243zf) + isobutane (R600a) at temperatures from 283.15 to 323.15 K," *International Journal of Refrigeration,* no. 161, pp. 62-70, 2024.

[17] A. Jager, I. H. Bell and C. Breitkopf, "A theoretically based departure function for multi-fluid mixture models," *Fluid Phase Equilibria,* no. 469, pp. 56-69, 2018.

[18] M.-J. Huron and J. Vidal, "New mixing rules in simple equations of state for representing vapour-liquid equilibria of strongly non-ideal mixtures," *Fluid Phase Equilibria,* pp. 255-271, 1979.

[19] D. S. Abrams and J. M. Prausnitz, "Statistical Thermodynamics of Liquid Mixtures: A New Expression for the Excess Gibbs Energy of Partly or Completely Miscible Systems," *AIChE journal,* vol. 21, no. 1, pp. 116-128, 1975.

[20] B. Schmid and J. Gmehling, "Revised parameters and typical results of the VTPR group contribution equation of state," *Fluid Phase Equilibria,* vol. 317, pp. 110-126, 2012.

[21] I. Bell, E. Mickoleit, C.-M. Hsieh, S.-T. Lin, J. Vrabec, C. Breitkopf and A. Jäger, "A Benchmark Open-Source Implementation of COSMO-SAC," *Journal of Chemical Theory and Computation,* vol. 16, no. 4, 2020.

[22] F. W. Dittus and L. M. K. Boelter, "Heat transfer in automobile radiators of the tubular type," *University of California Publications in English,* pp. 443-461, 1930.

[23] E. Sieder and G. E. Tate, "Heat transfer and pressure drop of liquids in tubes," *Industrial & Engineering Chemistry,* vol. 28, no. 12, pp. 1429-1435, 1936.

[24] B. S. Petukhov, "Heat Transfer in a Single-Phase Medium under Supercritical Conditions," *Teplofizika Vysokikh Temperatur,* vol. 6, no. 4, pp. 732-742, 1968.

[25] V. Gnielinski, "New Equation for Heat and Mass Transfer in Turbulent Pipe and Channel Flow," *Int. Chem. Engg,* vol. 16, pp. 359-368, 1976.

[26] N. Kline, F. Feuerstein and S. Tavoularis, "Onset of heat transfer deterioration in vertical pipe flows of CO2 at supercritical pressures," *International Journal of Heat and Mass Transfer,* vol. 118, pp. 1056-1068, 2018.

[27] K. Yamagata, K. Nishikawa, S. Hasegaw, T. Fujii and S. Yoshida, "Forced convective heat transfer to supercritical water flowing in tubes," *International Journal of Heat and Mass Transfer,* vol. 15, no. 12, pp. 2575-2593, 1972.

[28] S. Mokry, I. Pioro, P. Kirillov and Y. Gaspadinov, "Supercritical-water heat transfer in a vertical bare

This project has received funding from the European Union's Horizon Europe research and innovation program under grant agreement No 101083558

tube," *Nuclear Engineering and Design,* vol. 240, no. 3, pp. 568-576, 2010.

[29] X. Cheng, Y. H. Yang and S. F. Huang, "A simplified method for heat transfer prediction of supercritical fluids in circular tubes," *Annals of Nuclear Energy,* vol. 36, no. 8, pp. 1120-1128, 2009.

[30] G. A. Schatte, A. Kohlhepp, C. Wieland and H. Spliethoff, "Development of a new empirical correlation for the prediction of the onset of the deterioration of heat transfer to supercritical water in vertical tubes," *International Journal of Heat and Mass Transfer,* vol. 102, pp. 133-141, 2016.

[31] B. S. Shiralkar and P. Griffith, " The Deterioration in Heat Transfer to Fluids at Supercritical Pressure and High Heat Fluxes," *MIT Engineering Project Laboratory* , pp. 70332-70351, 1968.

[32] V. A. Grabezhnaya and P. L. Kirillov, "Heat transfer under supercritical pressures and heat transfer deterioration boundaries," *Thermal Engineering,* vol. 53, no. 4, pp. 296-301, 2006.

[33] J. D. Jackson, "Models of heat transfer to fluids at supercritical pressure with influences of buoyancy and acceleration," *Applied Thermal Engineering,* vol. 124, pp. 1481-1491, 2017.

[34] B. Zhu, J. Xu, X. Wu, J. Xie and L. Mingjia, "Supercritical "boiling" number, a new parameter to distinguish two regimes," *International Journal of Thermal Sciences,* vol. 136, pp. 254-266, 2019.

[35] H. Zhang, J. Xu and Q. Wang, "Determination of the position and characteristics of supercritical heat," *International Journal of Thermal Sciences,* vol. 188, 2023.

[36] J. Xie, D. Liu, H. Yan, G. Xie and S. K. S. Boetcher, "A review of heat transfer deterioration of supercritical carbon dioxide flowing in vertical tubes: Heat transfer behaviors, identification methods, critical heat fluxes, and heat transfer correlations," *International Journal of Heat and Mass Transfer,* vol. 149, 2020.

[37] M. M. Ehsan, Z. GUan and A. Y. Klimenko, "A comprehensive review on heat transfer and pressure drop characteristics and correlations with supercritical CO2 under heating and cooling," *Renewable and Sustainable Energy Reviews,* vol. 92, pp. 658-675, 2018.

[38] A. Alasif, A. Pucciarelli, O. Siddiqui and A. Shams, "An overview of the prediction methods for the heat transfer of supercritical fluids," *Progress in Nuclear Energy,* vol. 181, 2025.

[39] Z.-H. Li, P.-X. Jiang, C.-R. Zhao and Y. Zhang, "Experimental investigation of convection heat transfer of CO2 at supercritical pressures in a vertical circular tube," *Experimental Thermal and Fluid Science,* vol. 34, no. 8, pp. 1162-1171, 2010.

[40] H.-K. Oh and C.-H. Son, "New correlation to predict the heat transfer coefficient in-tube cooling of supercritical CO2 in horizontal macro-tubes," *Experimental Thermal and Fluid Science,* vol. 34, no. 8, pp. 1230-1241, 2010.

This project has received funding from the European Union's Horizon Europe research and innovation program under grant agreement No 101083558

7. Annex I: Assessment of EoS for Mixture Modelling

The first important point in modelling mixtures is the substantial difference between systems in which the components are completely miscible—allowing the mixture to be treated as a single phase with a single equation of state—and systems with immiscible components, which require a more complex description of their fluid dynamic behaviour. For the latter case, preliminary results from the measurements obtained in Task 3.1 suggest that ionic liquids do not completely dissolve in CO_2, resulting in the presence of liquid droplets entrained within the main CO_2 flow.

As already stated in Dr. Ungar's PhD Thesis [4], the model developed by UNIFI (*BHEModel2.0*) is based on a 1D version of the momentum and energy balance equations, which is integrated over the well length to predict the pressure and temperature profile of the fluid:

$$\frac{dp}{dl} = -(\rho g cos\theta + dp_{loss}) \tag{7}$$

$$\frac{dh}{dl} = -\left(gcos\theta + \frac{d\dot{q}_{tot}}{\dot{m}_{well}}\right) \tag{8}$$

With the real model actually integrating over density, exploiting a relation retrieved using the fluid EoS:

$$\frac{d\rho}{dl} = \left(\frac{\partial\rho}{\partial p}\Big|_T + \frac{\partial\rho}{\partial T}\Big|_p \frac{\frac{dh}{dp} - \frac{\partial h}{\partial p}\Big|_T}{\frac{\partial h}{\partial T}\Big|_p}\right)\frac{dp}{dl} \tag{9}$$

The term dh/dp is evaluated by dividing the results from Eqs. (7) and (8). All the partial derivatives highlighted in blue in Eq. (9) are evaluated from the EoS (REFPROP directly provides them given the fluid state). Finally, the two terms dp_{loss} and $d\dot{q}_{tot}$ must be evaluated with specific correlations.

In the following sections, we describe how the previous model has been modified to account for both mixture modelling scenarios**Error! Reference source not found.** Figure **13** gives an overview of the fluid modelling approach implemented by UNIFI in its code for simulating well behaviour.

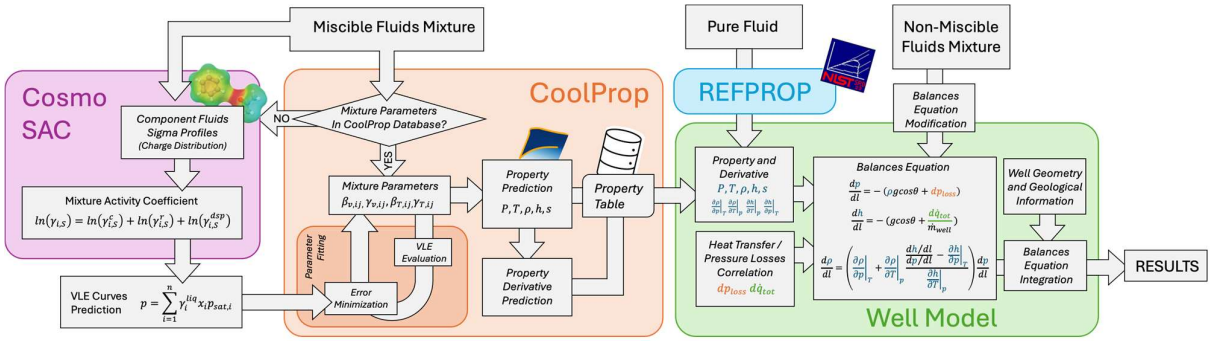

*Figure **13.** - Scheme of the UNIFI approach for modelling mixtures*

This project has received funding from the European Union's Horizon Europe research and innovation program under grant agreement No 101083558

7.1. Miscible Fluids Mixture Model

7.1.1. General Introduction

For completely miscible mixtures, equations (7) – (9) remain valid and can be applied to describe fluid behaviour in the well. The main difference with respect to pure fluids lies in the underlying EoS, which must be adapted. This adaptation is implemented in fluid property solvers such as REFPROP and CoolProp, which in turn are mainly based on Helmholtz Energy-based EoS, through the introduction of *binary interaction parameters* (BIP) for each pair of mixture components. These parameters are incorporated into the departure function for the Helmholtz energy of the mixture, from which all other thermodynamic properties can be derived [14].

BIPs are typically determined experimentally by fitting EoS predictions to accurate vapor–liquid equilibrium (VLE) measurements, as demonstrated, for example, by Bell and Lemmon [15] and by Menegazzo et al. [16]. In recent years, REFPROP and CoolProp have served as informal centralized repositories, collecting, validating, and disseminating evaluated interaction parameters published in the literature.

However, the evaluation of BIPs is limited by two factors: (i) the complexity of the experimental apparatus required, and (ii) the rapid increase in the number of parameters, since each fluid pair requires its own value. As a result, only a limited set of mixtures has experimentally determined parameters. Moreover, while Helmholtz-energy-based EoS provide excellent accuracy once BIPs are known, they exhibit poor predictive capability for mixtures with unknown coefficients, as pointed out by Jäger et al. [17].

To overcome these limitations and enable predictions for mixtures without experimentally determined BIPs, theoretical methods have been developed to approximate the parameters from molecular structure.

The first approach was originally proposed in the late 1970s at IFPEN by Huron and Vidal [18], who combined cubic EoS with fugacity and excess Gibbs free energy models. Since excess Gibbs energy can be obtained from statistical mechanics [19], their method significantly improved predictive performance. However, its accuracy remained constrained by the intrinsic limitations of cubic EOS.

Building on this idea, Jäger, Bell, and Breitkopf [17] proposed a model coupling Helmholtz-energy-based EoS with excess Gibbs free energy models, enabling accurate property predictions for fluid mixtures. Although excess Gibbs energy correlations still require experimental input, these parameters are more transferable than BIPs: they can be fitted to molecular groups or subgroups and then used to predict the behaviour of mixtures containing related fluids [20].

The latest developments combine Gibbs free energy methods with quantum-mechanical models of molecular interactions, notably the conductor-like screening model (COSMO). COSMO first estimates the charge distribution on each molecule, based on atomic structure, generating so-called sigma-profiles—probability distributions of surface charge densities. These profiles are then used to estimate intermolecular interactions by averaging over all possible relative orientations of molecular surface segments. The resulting interaction energies are directly employed to evaluate activity coefficients, fugacity, and ultimately to predict VLE behaviour. [21]

7.1.2. UNIFI Modelling Approach

Building on the results of the literature review, different models with an increasing level of accuracy and complexity have been implemented in the UNIFI code. An overview of these methods is illustrated in Figure 14.

This project has received funding from the European Union's Horizon Europe research and innovation program under grant agreement No 101083558

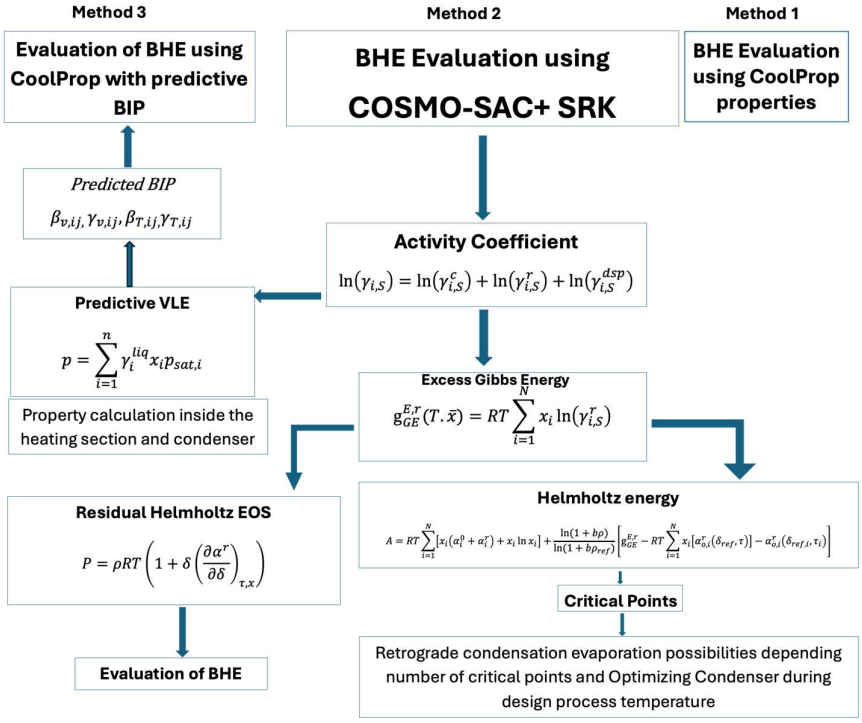

*Figure **14.** - Possible methods for modelling mixtures*

The first and simplest option (Method 1) is to directly use REFPROP or CoolProp, provided that the binary interaction parameters (BIPs) for the selected mixture are available in their databases. However, even in this case, the higher complexity of the underlying EoS leads to reduced code stability and fewer flash calculation options compared with the pure fluid case. For this reason, CoolProp is not directly called within the code; instead, it is used to generate property tables, which are then interpolated using the SciPy interpolation libraries.

When BIPs are not available for the mixture of interest, two alternative modelling approaches have been developed.. Method 2 follows the methodology described by Bell and colleagues, which employs the open-source COSMO-SAC model to generate sigma profiles and predict activity coefficients. These results are then used in an in-house Helmholtz-based EoS calculator to evaluate mixture performance. This method is more direct but requires the development of a dedicated EoS solver, since standard solvers such as CoolProp and REFPROP do not allow direct specification of the excess Gibbs free energy in their formulations. Consequently, this approach has been applied mainly to simplified well models, where only a limited set of properties is needed, or to specific parameter evaluations such as the critical point. For more complex cases, the COSMO-SAC–predicted activity coefficients have instead been used to generate VLE data (Method 3), which are then employed to fit the BIPs following the method proposed by Bell [15]. These fitted parameters can be included in CoolProp, thereby enabling the use of a robust and relatively stable solver for thermodynamic property evaluation.

This project has received funding from the European Union's Horizon Europe research and innovation program under grant agreement No 101083558

7.2. Non-Miscible Fluids Mixture Model

Models for multiphase fluids have been extensively studied due to their wide range of applications. In this work, we focus on particle-laden flows, a class of two-phase systems characterised by a continuous carrier phase (typically a liquid or gas) that transports a dispersed phase of small, immiscible particles. These particles can represent ionic liquid droplets or nanoparticles added to enhance heat transfer. Such models are inherently complex, as they must account for interphase interactions such as drag forces, as well as heat and mass transfer between phases. In the scope of the current analysis, an **"Ideal" Mixture** model has been implemented.

This simplified model is based on several assumptions, such as:

- The particles (or droplets) are carried along with the fluid at a speed equal to the speed of the fluid flow
- The particles (or droplets) are in thermal equilibrium with the fluid
- The particles do not interact with each other

These assumptions are usually correct for very small droplets and for low concentrations and can be useful to obtain a simple and reliable model for a preliminary estimation, even when these conditions are not strictly met.

Under these assumptions, the mass concentration of the droplet is the same in every section of the pipe, and the effect of the presence of the fluid on the energy equation actually reduces to a change in the fluid's specific heat (Cp).

Keeping in mind that our goal is to obtain a correlation to modify Eqs. (7) to (9), we can state the following:

- The density of the mixture is defined as a volume-averaged mean of the density:

$$\rho_{mix} = \rho_p \Phi + \rho_f (1 - \Phi) \tag{10}$$

Which is an implicit formulation, because the volumetric fraction of the particle Φ changes with the density of the fluid. To account for this, we must include the definition of the mass fraction w as a function of particles and gas volumes and densities:

$$w = \frac{m_p}{m_p + m_f} = \frac{\rho_p V_p}{\rho_p V_p + \rho_f V_f} = \frac{\rho_p \Phi}{\rho_p \Phi + \rho_f (1 - \Phi)} \tag{11}$$

Combining (10) and (11), after some manipulation, it is possible to obtain:

$$\rho_{mix} = \frac{1}{1 - \mathrm{w}\left(1 - \frac{\rho_f}{\rho_p}\right)} \rho_f \tag{12}$$

The derivative of the density can be evaluated from Eq. (6), considering that w is constant:

$$d\rho_{mix} = \frac{d\rho_{mix}}{d\rho_f} d\rho_f = \frac{1 - \mathrm{w}}{\left(1 - \mathrm{w}\left(1 - \frac{\rho_f}{\rho_p}\right)\right)^2} d\rho_f \tag{13}$$

Further, it must be noted that the volumetric fraction becomes:

$$\Phi = \frac{1}{1 + \frac{\rho_p}{\rho_f}\frac{1 - w}{w}} \tag{14}$$

This project has received funding from the European Union's Horizon Europe research and innovation program under grant agreement No 101083558

That should be used in the evaluation of the speed to be included in the evaluation of pressure losses:

$$\mathrm{u} = \frac{\dot{m}_f}{\rho_f A(1-\Phi)} \tag{15}$$

- Similarly, the enthalpy of the mixture is defined as a mass-averaged mean of the enthalpy:

$$h_{mix} = h_p \mathrm{w} + h_f(1-\mathrm{w}) = \mathrm{c_{p}}_p T\, w + h_f(1-\mathrm{w}) \tag{16}$$

From which:

$$c_{p_{mix}} = \left.\frac{\partial h_{mix}}{\partial T}\right|_p = \mathrm{c_{p}}_p w + \mathrm{c_{p}}_f(1-\mathrm{w}) \tag{17}$$

And:

$$\left.\frac{\partial h_{mix}}{\partial T}\right|_p = \left.\frac{\partial h_f}{\partial T}\right|_p (1-\mathrm{w}) + \mathrm{c_{p}}_p w \tag{18}$$

$$\left.\frac{\partial h_{mix}}{\partial p}\right|_T = \left.\frac{\partial h_f}{\partial p}\right|_T (1-\mathrm{w}) \tag{19}$$

- The same applies for the pressure that, for the mixture, is equal to the sum of the partial pressures of the components, hence:

$$p_{mix} = \frac{1}{1-\Phi} p_f \tag{20}$$

$$dp_{mix} = \frac{1}{1-\Phi} dp_f = \frac{1-w\left(1-\frac{\rho_f}{\rho_p}\right)}{1-w} dp_f \tag{21}$$

Finally, using the relations just derived, we can adapt Eqs. (7) to (9) to derive the final model to be integrated.

$$\frac{dp_f}{dl} = -\frac{1-\mathrm{w}}{\left[1-\mathrm{w}\left(1-\frac{\rho_f}{\rho_p}\right)\right]^2}\left(\rho_f g cos\theta + \left[1-\mathrm{w}\left(1-\frac{\rho_f}{\rho_p}\right)\right] dp_{loss}\right) \tag{22}$$

$$\frac{dh_{mix}}{dl} = -\left(g cos\theta + (1-\mathrm{w})\frac{d\dot{q}_{tot}}{\dot{m}_f}\right) \tag{23}$$

$$\frac{d\rho_f}{dl} = \left(\left.\frac{\partial \rho_f}{\partial p}\right|_T + \left.\frac{\partial \rho_f}{\partial T}\right|_p \frac{\frac{dh_{mix}}{dp_f} - (1-\mathrm{w})\left.\frac{\partial h_f}{\partial p}\right|_T}{(1-\mathrm{w})\left.\frac{\partial h_f}{\partial T}\right|_p + \mathrm{c_{p}}_p w}\right)\frac{dp_f}{dl} \tag{24}$$

It must be remarked that, after rewriting, the overall shape of the equations remains the same with only the inclusion of some modifiers to account for the presence of the particles (highlighted in violet). Therefore, the overall solution procedure of the system is completely unaffected.

This project has received funding from the European Union's Horizon Europe research and innovation program under grant agreement No 101083558

8. Annex II: Analysis of Heat Transfer Coefficients for Supercritical Flows

The modelling of the heat transfer coefficient for trans-critical and supercritical flows represents one of the most challenging aspects in heat transfer applications. For single-phase subcritical fluids, all the thermodynamic and transport properties (density, specific heat, viscosity, thermal conductivity and Prandtl number) experience limited variations with pressure and temperature. This condition proved to be extremely beneficial from a modelling point of view for both laminar and turbulent regimes and many correlations have been developed to fit experimental data. Starting from the pivotal work of Dittus and Boelter (1930) [22], which developed a correlation to predict the heat transfer coefficient through non-dimensional analysis as:

$$Nu = 0.023 Re^{0.8} Pr^{0.4} \quad (19)$$

several well-known correlations have been proposed to target a specific flow regime or to extend the range of application. Sieder and Tate (1936) [23] introduced a correction on the viscosity to account for applications where high temperature differences are experienced. Petukhov (1970) [24] and Gnielinski (1976) [25] proposed more detailed semi-empirical models to extend the range of validity in terms of Reynolds and Prandtl numbers.

These correlations, however, lose accuracy when dealing with a two-phase regime. When saturation conditions are encountered, an abrupt change in thermodynamic properties occurs when transitioning from vapour to liquid or vice versa, resulting in highly complex fluid structures.

At supercritical pressure, a clear distinction between single-phase and two-phase regimes cannot be made. Nevertheless, the thermodynamic properties change significantly near the so-called pseudo-critical line (also known as Widom line or pseudo-boiling line), which represents the locus of points where the temperature corresponds to the maximum specific heat at a given pressure. At the vicinity of this line, the fluid shows rapid and nonlinear variations in its physical properties, as shown in Figure **15** for sCO_2.

This project has received funding from the European Union's Horizon Europe research and innovation program under grant agreement No 101083558

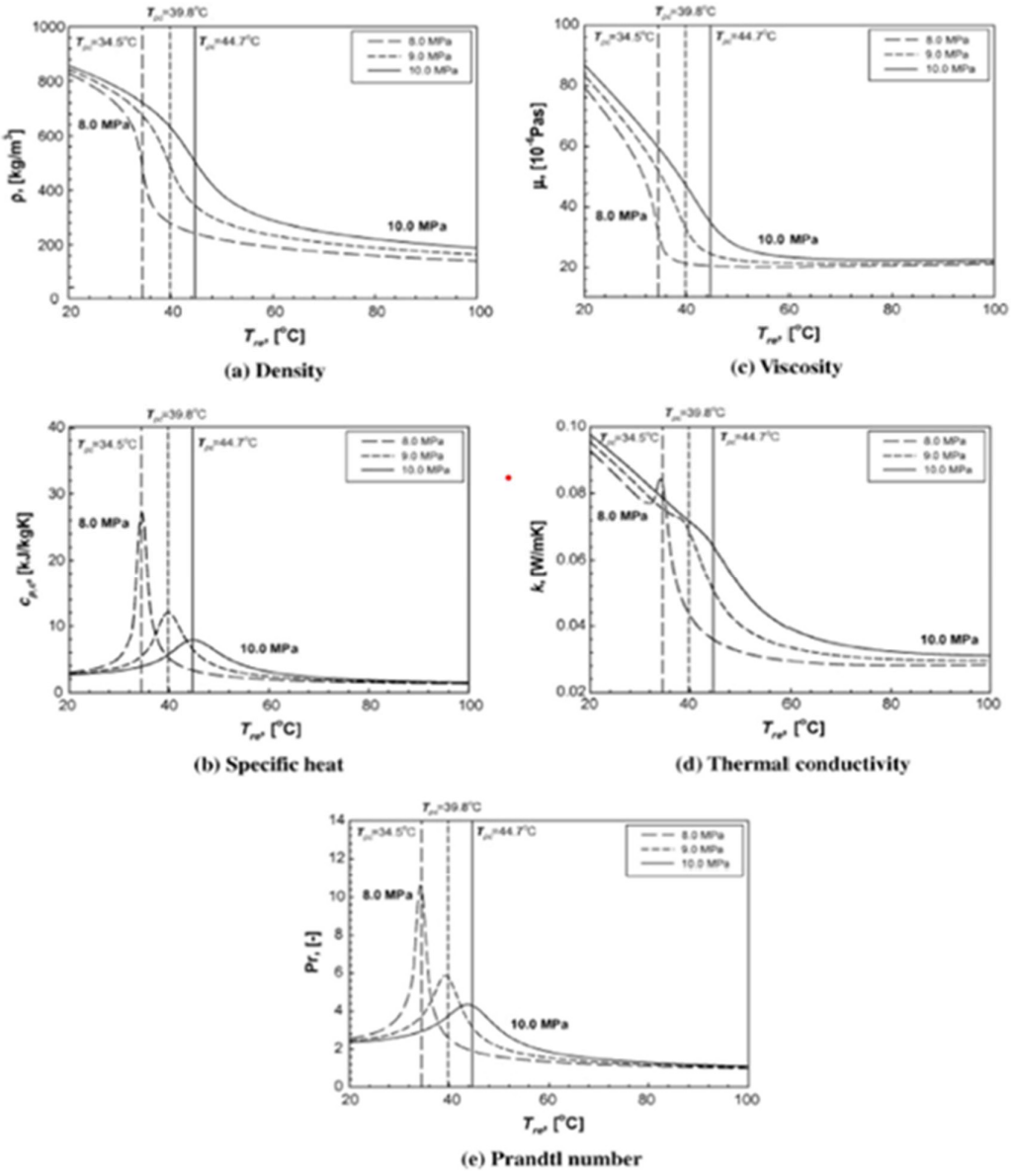

*Figure **15.** Physical property variation of sCO2 as a function of temperature and pressure [40]*

With increasing operating pressure, the pseudocritical temperature rises, and the variation in thermophysical properties becomes less pronounced. However, as the operating pressure approaches the critical pressure, each property undergoes a rapid and significant change near the pseudocritical temperature.

Wrapping up, supercritical flows should be considered as single-phase substances, although they can be distinguished into gas-like or liquid-like flows, depending on whether the temperature is lower or higher than the pseudocritical value. Moreover, crossing the pseudocritical line has an analogy with an evaporation/condensation process, even if the slope of the property variations is strongly reduced. For this reason, the heat transfer performances can deviate significantly from those of classic single-phase turbulent flows. Three major heat transfer regimes are normally identified for supercritical flows:

This project has received funding from the European Union's Horizon Europe research and innovation program under grant agreement No 101083558

- **Normal Heat Transfer**: it consists of a trend for the heat transfer coefficient that is similar to that of a classic subcritical flow. Therefore, heat transfer parameters can be evaluated starting from the typical correlations for turbulent flows (with, at most, a few minor corrections).
- **Enhanced Heat Transfer**: it consists of a trend for the heat transfer coefficient where the actual heat transfer is enhanced because of the fluid interaction with the wall.
- **Deteriorated Heat Transfer**: it consists of a trend for the heat transfer coefficient where the actual heat transfer is reduced because of the fluid interaction with the wall.

An example of the different regimes is presented in Figure **16**, where two different heat fluxes are applied to supercritical CO_2 flowing in a pipe.

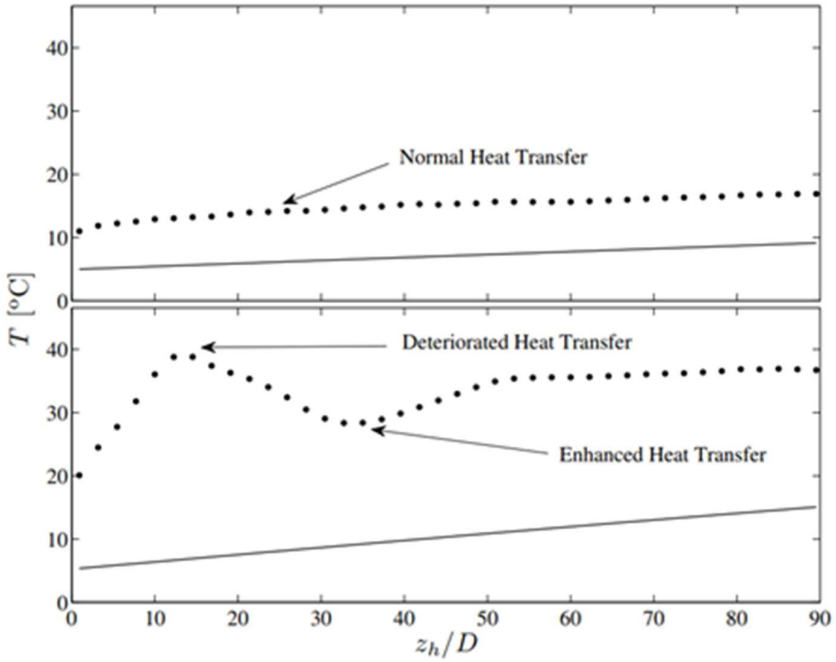

*Figure **16.** Temperature distribution along a non-dimensional axial coordinate (z_h = length, D = diameter) of a pipe in different heat transfer regimes for sCO_2. Solid line for bulk temperature, dashed line for wall temperature [26]*

The intensity of the temperature peak can be drastically different from the one reported in the previous figure, therefore leading to several issues, such as "hot spots" or temperature imbalances. Even though this issue is particularly relevant in other scientific fields (like supercritical nuclear water reactors) where wall heat fluxes are extremely high, it should be noted that this phenomenon could also occur for geothermal applications once a given combination of geothermal gradient and geometry of the pipe is achieved. Consequently, a prediction of the occurrence of this phenomenon becomes essential to obtain a proper design for a sCO_2 borehole.

Although the cause of these particular trends is arguably the difference in density between the fluid close to the wall and the one in the bulk, the scientific community has been struggling since the 1950s to find a way to predict both the occurrence of this phenomenon and its intensity, especially for the deteriorated regime. In the following sections, a quick overview of the approaches proposed over the last years will be provided.

This project has received funding from the European Union's Horizon Europe research and innovation program under grant agreement No 101083558

However, it is important to highlight that a comprehensive model for the characterization of the heat transfer in supercritical applications is still not available, as the majority of the proposed approaches appear to be case sensitive and valid only in a limited range of applications. For this reason, the following correlations/models should be considered as a reference for the development of a new correlation for the heat transfer coefficient in an HOCLOOP system for supercritical CO_2. A proper refinement and calibration of this correlation will be performed once the experimental data from Task 3.1 are available.

8.1. Heat Transfer Deterioration (HTD)

In the supercritical region, the significant variations in the thermophysical properties of the fluid lead to a substantial dependence of the heat transfer coefficient on the local bulk temperature, heat flux, and tube diameter. This peculiarity of supercritical flows is prone to cause HTD, generally defined as an abnormal increase of the local wall temperature and correspondingly sharp reduction of the heat transfer coefficient. The extremely high temperatures may exceed the limiting temperature of the tube material and reduce the heat transfer efficiency.

Since the earlier experimental occurrences of this phenomenon, one of the main focuses for the scientific community has been to establish a set of heat transfer conditions (mass flow rate, wall heat flux, geometry and pressure) for it to occur. Therefore, numerous studies have proposed different criteria for the evaluation of a threshold value that could be used to predict the onset of this deterioration during design procedures.

Although the objective of all these studies is the same, the procedures developed to identify this threshold value have followed very different approaches.

From a historical point of view, due to the complexity of the phenomena originating this deterioration, many authors have preferred to define some *"empirical"* correlations, based on the classic heat transfer applications parameters (mass flow rate, tube diameter, heat flux...), rather than some "*theoretical*" ones. The basic idea for these correlations is to identify the threshold value as the heat flux q_{onset} that corresponds to the onset of HTD. Despite the various parameters that normally affect the heat transfer coefficient, most of the correlations define q_{onset} simply as a power function of mass flux G:

$$q_{onset} = mG^n \tag{20}$$

where $G = \dot{m}/A$ represents the mass flow rate per unit of sectional area.

Although these power laws appear to provide a good estimate, many authors have proposed different values for m and n, depending on the channel shape and type of fluid. Over the years, other authors have suggested different relationships between q_{onset} and G, such as a linear relationship or the inclusion of correction factors for pressure or tube diameter. Anyway, even if the accuracy could be slightly higher or slightly lower for a given application, all these correlations appear to give approximately the same order of magnitude for the threshold parameter. The most relevant correlations are summarised in Table 12.

This project has received funding from the European Union's Horizon Europe research and innovation program under grant agreement No 101083558

Table 12. Heat Transfer Deterioration Prediction Correlations

Reference	HTD Onset Correlation	Fluid	P (MPa) / G (kg/(m2s) /d (mm)
Yamagata et al. [27]	$q_{onset} = 0.2G^{1.2}$	Water	22.6-31 / 310-1830 /8-10
Mokry et al. [28]	$q_{onset} = -58.97 + 0.745\,G$	Water	24 / 200 – 1500 / 10
Cheng et al. [29]	$q_{onset} = 0.001354 * F * G$ $F = \frac{c_{p,pc}}{\beta_{pc}}$	Water	22.5 – 31 / 500-3600 / 2.5 - 20
Schatte et al. [30]	$q_{onset} = 1.942 * 10^{-6}\,(30-d)^{0.339} F^{2.065} G^{0.795}$ $F = \frac{c_{p,pc}}{\beta_{pc}}$	Water	22.5–30/203–1500/7.5–26
Shiralkar et al. [31]	$q_{onset} = 0.00316G^{1.495}$	CO_2	7.93 / 830-2508 / 6.34
Grabheznaya et al. [32]	$q_{onset} = 0.6\ M_{water}/M\ G$	Water, CO_2	-- / 250-1500 / --
Kline et al. [26]	$q_{onset} = 0.0002 * F * G^2$ $F = 0.7 + (1-0.7)/\left(1 + e^{4(d/d_{ref}-2.35)}\right)$	CO_2	8.336 / 300-1500 / 4.6 - 22

Another approach to distinguishing HTD from normal heat transfer cases involves evaluating the buoyancy and acceleration parameters. Jackson et al. [33] investigated the influence of buoyancy by plotting the reduced Nusselt number against the buoyancy parameter within the same coordinate system. Their analysis suggested that HTD cases could be identified based on the calculated buoyancy parameters; however, this criterion was applicable only in situations where the influence of other factors could be neglected.

More recently, Zhu et al. [34] proposed a general criterion by exploiting the analogy between subcritical boiling and supercritical "boiling" and introducing a supercritical "boiling" number (SBO). Starting from the non-dimensional subcritical boiling number (Bo), defined as:

$$Bo = q_{onset}/Gh_{lv} \quad (21)$$

the authors introduced a correction to extend this parameter to supercritical conditions, substituting the phase transition enthalpy value (h_{lv}) with the enthalpy value at the pseudo-critical point (h_{pc}).

$$SBO = q_{onset}/Gh_{pc} \quad (22)$$

A threshold value of SBO=5.126*10^{-4} was found to agree with a wide range of sCO2 experimental data. Zhang et al. [35] extend this approach to different fluids as water, R22 and R134a.

8.1.1. Heat Transfer Coefficient Correlations

As mentioned in the previous section, the conventional correlations of turbulent forced convection for

This project has received funding from the European Union's Horizon Europe research and innovation program under grant agreement No 101083558

constant property fluids failed to predict the heat transfer mechanisms once the critical condition is approached. Starting from those correlations, researchers proposed two methods to incorporate the effects of the temperature-dependent thermodynamic properties of supercritical fluids.

In the *Reference Temperature* method, all the thermodynamic properties are generally calculated at the mean bulk fluid temperature (or at the mean wall temperature). This approach proved to be very effective in keeping the solution as simple as possible and in reducing the computational cost, but generally, they were reported to be less efficient.

The most widely used method is the so-called *Property Ratio* method, where the ratio of properties calculated at bulk fluid and wall temperature is included in the correlation. This is particularly interesting for including the effect of the properties that exhibit extremely rapid variation near the pseudocritical temperature incorporated in the turbulent forced convection heat transfer correlation.

For the sake of brevity, a review of the various heat transfer correlations is not reported in this document. A complete summary can be found in [36] [37]. However, a general conclusion is that the tested correlations show considerable disagreement with the experimental data in their studies. No correlation can predict the heat transfer well over wide parameter ranges, especially when HTD occurs.

8.2. CFD Approaches

Computational Fluid Dynamics (CFD) has recently been employed to model heat transfer in supercritical fluids; however, satisfactory results have yet to be achieved. Three primary approaches are available for implementing CFD. The most widely adopted is the Reynolds-Averaged Navier–Stokes (RANS) simulation, whose principal advantage is the relatively low computational cost, as all turbulence scales are modelled. Nevertheless, this method is also the least accurate, particularly for supercritical fluids. Large Eddy Simulation (LES) and Direct Numerical Simulation (DNS) are applied less frequently than RANS due to their substantially higher computational demands.

When focusing on RANS approaches, substantial discrepancies between numerical predictions and experimental observations are frequently reported in the analysis of heat transfer deterioration [38]. Depending on the selected turbulence model, this phenomenon may be either underestimated or overestimated, resulting in markedly different and often unreliable predictions of the temperature field. Moreover, a wide range of turbulence models (e.g., k–ε, RNG k–ε, k–ω, SST k–ω) has been employed across various studies, highlighting the absence of a universally preferred model for fluids in the supercritical phase. This underscores the need for further modelling development before CFD can be regarded as a reliable tool for predicting the heat transfer in supercritical fluids.

To have a proper estimation of the performance of these models in supercritical fluid heat transfer applications, a specific case study has been analysed [39]. An assessment of the most widely used turbulence models is presented in the following subsection.

8.2.1. CFD Assessment

The main features of the experimental test case are summarised in Table 13

Table 13. Experimental Testcase Main Features

Fluid	CO_2
Pressure	88 bar

This project has received funding from the European Union's Horizon Europe research and innovation program under grant agreement No 101083558

Mass Flux	325 kg/(m^{2}s)
Heat Flux	39 kW/m^2
Length (Vertical)	0.29 m
Inlet Temperature	25°C
Diameter	0.002 m

Leveraging the physical and geometric symmetry of the experimental setup, a 2D axisymmetric domain has been adopted to reduce the computational cost. A representation of the numerical domain, including the specification of the boundary conditions, is shown in Figure 17

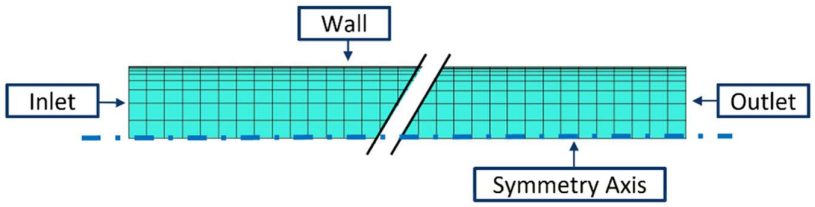

Figure 17. Numerical domain and boundary conditions

The static pressure is specified at the outlet section of the domain, while a constant heat flux is applied at the wall. To avoid spurious effects close to the inlet section, a fictitious unheated section has been added on the inlet side. Additionally, profiles of both velocity and the turbulence parameters have been specified at the inlet section. These profiles have been derived by patching the outlet profiles of a previous adiabatic simulation.

Numerical simulations were performed using the commercial solver ANSYS Fluent 2021 R1, based on the finite volume scheme. A SIMPLE scheme was used for coupling the pressure and velocity fields. Second-order upwind schemes have been used for all the transport variables.

Mesh sensitivities have been conducted for the different turbulence models. The primary focus of this analysis was on refining the mesh sizing in the radial direction, as the effect of sizing in the axial direction proved to be almost negligible. The proper meshes for the different turbulence models have been selected as the ones assuring the correct y^+ value at the first node from the wall.

To account for the extreme variation of the thermodynamic properties of the fluid in proximity of the critical point, the fluid properties have been calculated through the NIST database available in the ANSYS package. Since referring directly to the NIST database could increase the computational time, a lookup table has been created and used for the calculations. The number of points for the lookup table has been increased until the discrepancy of the properties was negligible with respect to the NIST EoS value, as shown in Figure 18.

This project has received funding from the European Union's Horizon Europe research and innovation program under grant agreement No 101083558

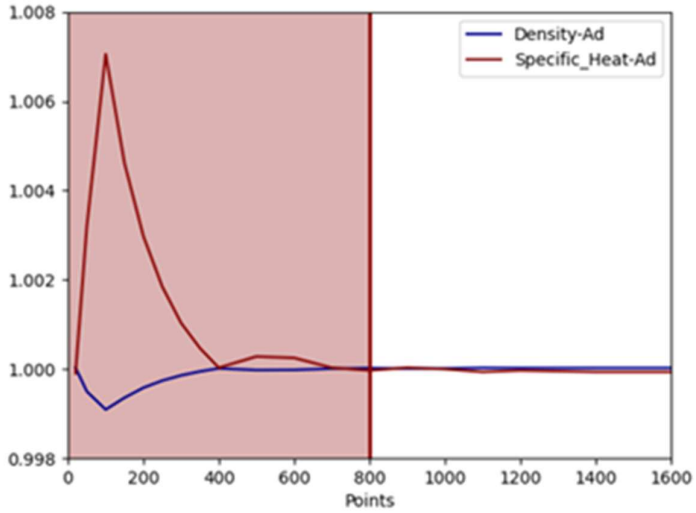

*Figure **18.** Lookup Table Sensitivity Analysis*

Three different turbulence models have been considered: a k–ε with Enhanced Wall Treatment, an SST k, and a k-kl–ω, which is a 3-equation transitional model. The result of the preliminary analysis is shown in Figure 19.

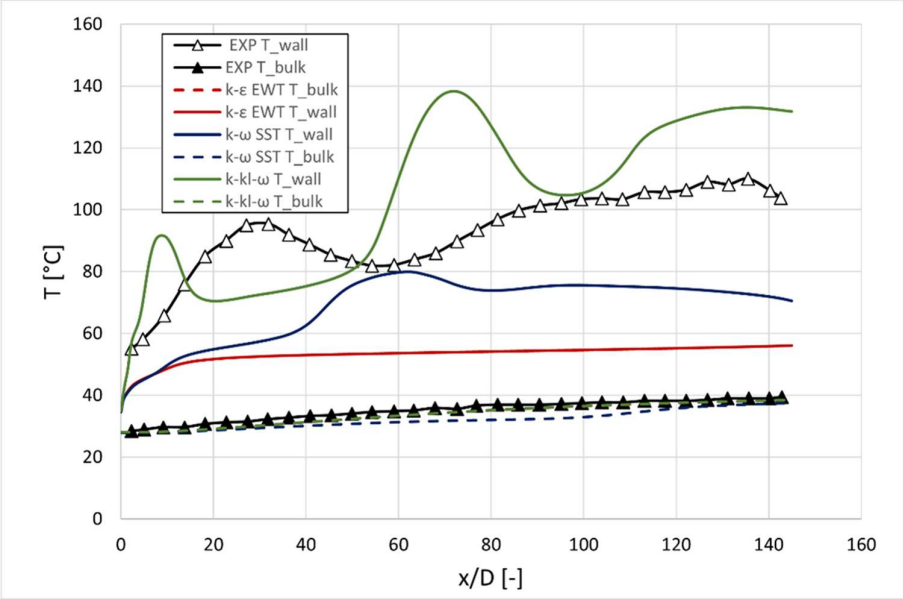

*Figure **19.** Preliminary CFD Assessment*

It appears that none of the previously proposed models is able to accurately reproduce the wall temperature trends observed in the experimental results. In particular, the k–ε model fails to predict the occurrence of heat transfer deterioration, while the SST k–ω model tends to underestimate the peak intensity and to predict its location with some delay. The transition model emerges as the most promising alternative, as it seems capable of at least capturing the onset of HTD. Nevertheless, it generally overpredicts the average wall temperature, while both the intensity and the position of the peak remain inaccurately represented.

This project has received funding from the European Union's Horizon Europe research and innovation program under grant agreement No 101083558

Overall, the experimentally observed wall temperature peak is not correctly reproduced, either in its magnitude or in its location. These findings indicate that, at the current stage, CFD cannot yet be considered a fully reliable tool for predicting the heat transfer mechanisms in supercritical flows. Although several modifications have been proposed in the literature to mitigate this limitation, their effectiveness remains strongly case-dependent. This underlines the need for further model development and systematic validation efforts to establish CFD as a robust predictive tool in this field.

This project has received funding from the European Union's Horizon Europe research and innovation program under grant agreement No 101083558